New Phytologist

Research

Unraveling mannan biosynthesis in poplar and spruce: functional characterization of Cellulose Synthase-Like family A (CSLA) genes

Sydne Guevara-Rozo[1,2], Lisanne de Vries[1,2], Yoshihisa Yoshimi[3], Elzat Eli[2], Paul Dupree[3] and Shawn D. Mansfield[1,2]

[1]Department of Wood Sciences, University of British Columbia, Vancouver, V6T 1Z4, Canada; [2]Department of Botany, University of British Columbia, Vancouver, V6T 1Z4, Canada; [3]Department of Biochemistry, University of Cambridge, Hopkins Building, The Downing Site, Tennis Court Road, Cambridge, CB2 1QW, UK

Author for correspondence:
Shawn D. Mansfield
Email: shawn.mansfield@ubc.ca

Received: *23 August 2025*
Accepted: *1 October 2025*

New Phytologist (2025)
doi: 10.1111/nph.70685

Key words: CSLAs, mannan, poplar, secondary cell wall, spruce.

Summary

- Hemicelluloses are key chemical constituents of plant cell walls, influencing structure, strength, and interactions between cellulose and lignin. While xylan has been widely studied and shown to affect cell wall integrity, the function of mannan remains largely unexplored. To address this gap, we identified and functionally characterized putative mannan biosynthetic genes from spruce and poplar, and tested their impact on wood formation and digestibility.
- Bioinformatic and phylogenetic tools were employed to identify Cellulose Synthase-Like family A (CSLA) genes from spruce and poplar. These genes were then functionally validated by complementing the mannan deficient Arabidopsis *csla2,3,9* triple mutants, and creating CRISPR-Cas9 knockouts and ectopic overexpression lines in poplar.
- Spruce and poplar CSLA candidates restored mannan biosynthesis in the Arabidopsis mutant. In poplar, mannan content was altered without impacting plant growth. Changes in mannan content marginally affected glucose and xylose release and improved cellulose hydrolysis during saccharification assays.
- This study demonstrates an effective approach to engineering mannan content in trees and highlights that this polysaccharide is not essential for cell wall formation in poplar. Our work provides a platform for further investigating the role of this polymer in tree cell wall structure and stability.

Introduction

Mannans are polymeric carbohydrates containing mannose as the principal constituent and are highly conserved through plant evolution. For example, they are the predominant cell wall polymer in several green algae, are highly abundant in the cell walls of early land plants such as mosses and lycophytes, and are also present in the cell walls of both gymnosperms and angiosperms (Rodríguez-Gacio *et al.*, 2012; Scheller & Ulvskov, 2010). Mannans play an essential role in plant embryonic development, as well as in maintaining seed mucilage architecture (Goubet *et al.*, 2009; Voiniciuc *et al.*, 2015). Recently, mannans have also been postulated to regulate the transition between primary and secondary cell wall deposition by acting as signal molecules (Zhao *et al.*, 2013; Zhang *et al.*, 2023). Mannans, similar to xylans, also interact and associate with other cell wall polymers in plant tissues to confer form and function (Yu *et al.*, 2022). Over the past few years, several studies have shown that mannans can bind directly to cellulose microfibrils and crosslink to lignin via ether bonds (Nishimura *et al.*, 2018; Terrett & Dupree, 2019). Although mannans have been widely studied in seed mucilage and primary cell walls (Yu *et al.*, 2014, 2018, 2022; Voiniciuc *et al.*, 2015), their role in plant secondary cell wall development and stability, and the genes responsible for their synthesis are still largely unknown in woody plants.

In the secondary cell wall, mannan abundance and composition differ markedly between gymnosperms and angiosperms (Scheller & Ulvskov, 2010; Terrett *et al.*, 2019; Berglund *et al.*, 2020). In gymnosperms such as spruce, galactoglucomannan predominates as the main hemicellulose, whereas in angiosperms like poplar, mannans are less abundant and xylan constitutes the majority of the hemicellulose content (Scheller & Ulvskov, 2010; Berglund *et al.*, 2020). These compositional variations likely reflect functional adaptations in cell wall structure and hydraulic efficiency across plant groups (Spicer, 2016). In gymnosperms, tracheids perform both water transport and mechanical support, functions that require the cell wall to be both flexible and tough, a role likely facilitated by the predominance of galactoglucomannan (Weng & Chapple, 2010; Spicer, 2016; Berglund *et al.*, 2020). By contrast, angiosperms evolved specialized vessels and fibres that separate these functions, coinciding with a shift from mannan to xylan, a polymer that binds tightly and uniformly to lignin and cellulose (Weng & Chapple, 2010; Spicer, 2016; Grantham *et al.*, 2017). This evolutionary divergence highlights the importance of studying

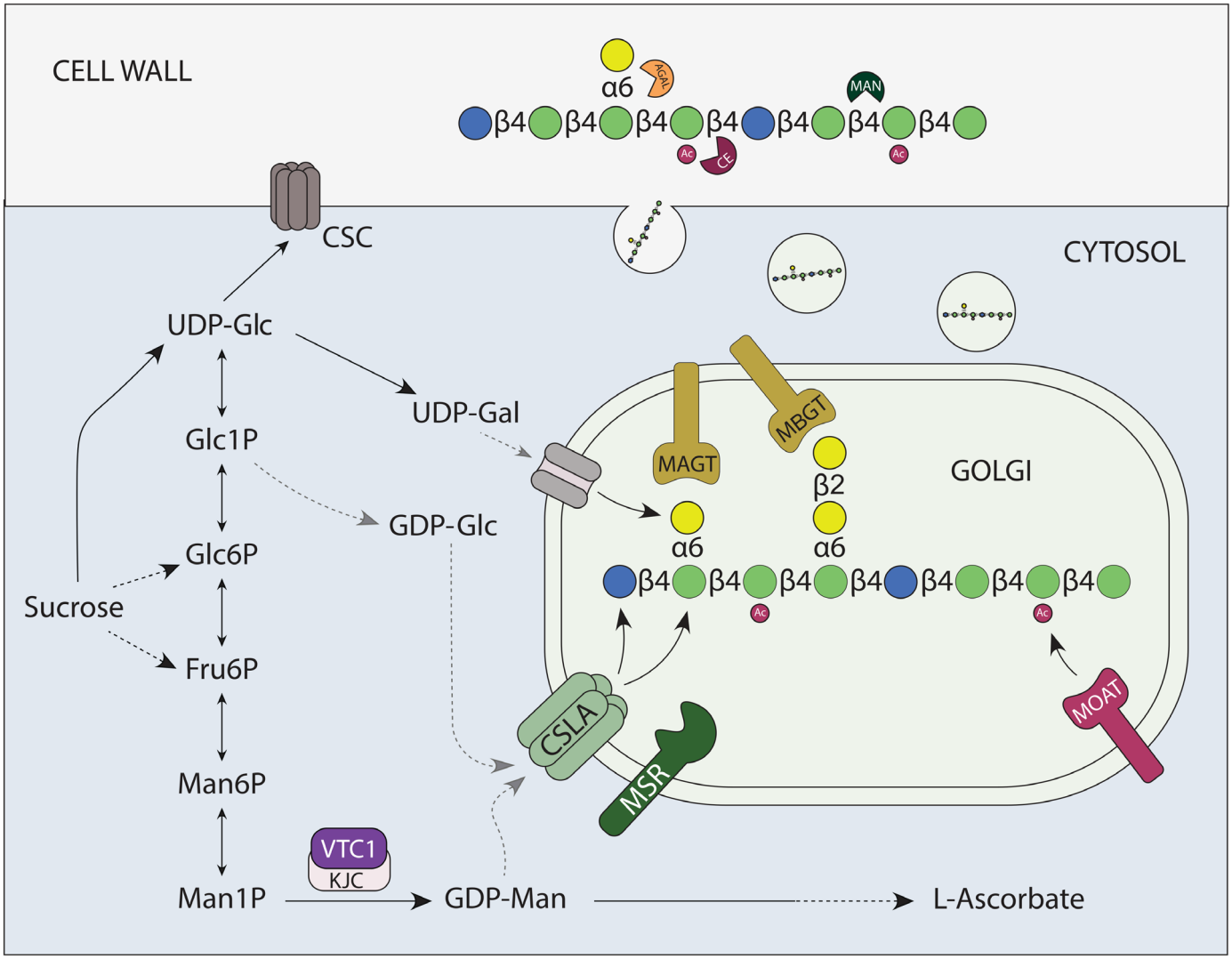

Fig. 1 Mannan biosynthesis. The substrate for mannan synthesis, Guanosine-Diphosphate-Mannose (GDP-Man), is synthesized in the cytosol by Mannose-1-Phosphate Guanylyltransferase/Vitamin C Defective I (GMP/VTC1) protein, whose enzymatic activity is stimulated by KONJAC (KJC) proteins (Conklin *et al*., 1999, 2000; Sawake *et al*., 2015). GDP-Man can either be used in the cytosol to produce ascorbic acid (Conklin *et al*., 1999, 2000) or transported to the Golgi to be used by Cellulose Synthase-Like A (CSLA) proteins as a substrate to synthesize the mannan backbone. CSLAs can also integrate GDP-glucose (GDP-Glc) into the sugar backbone to form glucomannan (Goubet *et al*., 2009; Voiniciuc, 2022). Mannan synthesis is further regulated by Mannan Synthesis-related proteins (MSRs; Wang *et al*., 2013; Voiniciuc *et al*., 2019), while additional modifications, including acetylation and galactosylation, are catalyzed by Mannan O-Acetyltransferases (MOAT1–MOAT4) and Mannan α- and β-Galactosyl Transferases (MAGT1/2, MBGT1), respectively (Zhong *et al*., 2018; Nishigaki *et al*., 2021; Yu *et al*., 2022). Following synthesis, mannans are transported to the extracellular matrix by exocytosis, where they undergo further remodeling by α-Galactosidases (AGAL), Carbohydrate Esterases (CE), and Mannanases (MAN; Edwards *et al*., 1992; Rodríguez-Gacio *et al*., 2012; Mai-Gisondi *et al*., 2017). CSC, Cellulose Synthase Complex. Green circles: mannose residues; blue circles: glucose residues; yellow circles: galactose residues; red circles: acetyl groups. Light gray dotted arrows indicate processes whose mechanisms are not fully understood. Black dotted arrows indicate that several steps are involved in the process.

factors that regulate mannan biosynthesis across different tree lineages. Therefore, this study focuses on gaining a deeper understanding of mannan biosynthesis in both poplar and spruce.

Mannan biosynthesis follows a multi-step pathway involving the formation of nucleotide sugars in the cytosol, polymerization of the mannan backbone in the Golgi, and subsequent addition of acetyl or galactosyl substitutions (Fig. 1; Scheller & Ulvskov, 2010; Voiniciuc, 2022). In Arabidopsis, Mannose-1-Phosphate Guanylyltransferase I/Vitamin C Defective I (GMP1/VTC1) is responsible for the synthesis of the nucleotide sugar Guanosine-Diphosphate-Mannose (GDP-Mannose) in the cytosol, a key precursor of mannan biosynthesis. The enzymatic activity of VTC1 is stimulated by the KONJAC (KJC1, KJC2) proteins (Conklin *et al*., 1999, 2000; Sawake *et al*., 2015). In the Golgi, GDP-Mannose as well as GDP-Glucose are used by Cellulose Synthase-Like family A (CSLA) proteins to catalyze the synthesis of mannan or glucomannan backbones (Goubet *et al*., 2009; Scheller & Ulvskov, 2010; Voiniciuc, 2022). Mannan synthesis is further regulated by Mannan Synthesis-Related proteins (MSRs; Voiniciuc *et al*., 2015; Wang *et al*., 2013), while additional modifications, including

acetylations and galactosylations, are catalyzed by Mannan O-Acetyltransferases (MOAT1–MOAT4) and Mannan α- and β-Galactosyl Transferases (MAGT1/2, MBGT1), respectively (Zhong *et al.*, 2018; Nishigaki *et al.*, 2021; Yu *et al.*, 2022). Following synthesis, mannans are transported to the extracellular matrix by exocytosis, where they undergo further remodeling by α-Galactosidases (AGAL), Carbohydrate Esterases (CE), and Mannanases (MAN; Edwards *et al.*, 1992; Mai-Gisondi *et al.*, 2017; Rodríguez-Gacio *et al.*, 2012).

In Arabidopsis, the CSLA gene family consists of nine members (*AtCSLA1–AtCSLA9*), with *AtCSLA7* being essential for embryo development and *AtCSLA2*, *AtCSLA3*, and *AtCSLA9* contributing to mannan biosynthesis in seed mucilage and stems (Goubet *et al.*, 2003, 2009). Arabidopsis *csla7* mutants are embryo lethal, arresting development at the globular stage and disrupting cell patterning and proliferation (Goubet *et al.*, 2003, 2009). In seeds, *csla2* mutants exhibited defects in mucilage architecture, with altered cellulose organization and reduced crystallinity (Yu *et al.*, 2014, 2018). Despite mannans being integral to early plant development, studies in the Arabidopsis *csla2,3,9* mutants suggest that their absence in secondary cell walls does not significantly impact plant growth (Goubet *et al.*, 2009). For example, in these Arabidopsis triple mutant plants, no major morphological changes or alterations in xylem mechanical strength were observed (Goubet *et al.*, 2009). In the perennial and fast-growing tree, poplar, five genes belonging to the CSLA family have been predicted to exist (*PtCSLA1–PtCSLA5*; Liepman *et al.*, 2005; Suzuki *et al.*, 2006), with two of them showing *in vitro* β-mannan synthase activity (*PtCSLA1* and *PtCSLA3*). However, none have been functionally characterized *in planta*.

Although Arabidopsis has been essential in uncovering aspects of secondary xylem development, tree species exhibit unique regulatory processes that cannot be fully elucidated in this model plant (Taylor, 2002; Lapierre *et al.*, 2021; De Meester *et al.*, 2022). For instance, the heterologous expression of DIKETIDE-CoA SYNTHASE (DCS) and CURCUMIN SYNTHASE 2 (CURS2) in Arabidopsis resulted in curcumin incorporation into lignified cell walls, enhancing saccharification efficacy without growth effects (De Meester *et al.*, 2022). However, in poplar, the same modifications led to altered growth phenotypes with no significant improvements in biomass digestibility (De Meester *et al.*, 2022). To better understand the role of mannans in secondary cell wall development, this study focuses on identifying and functionally characterizing CSLA genes in tree species. By manipulating their expression in poplar stems, we aim to elucidate how mannans contribute to cell wall architecture and integrity in trees. This research provides new insights into the molecular mechanisms governing cell wall formation in woody plants.

Materials and Methods

Identification of putative CSLAs

To identify putative functional CSLAs in poplar and spruce, sequences of CSLAs previously identified in Arabidopsis (*Arabidopsis thaliana* (L.) Heynh.) *AtCSLA2* (*AT5G22740*), *AtCSLA3* (*AT1G23480*), and *AtCSLA9* (*AT5G03760*) were used to complete BLAST searches against the poplar (*Populus trichocarpa* Torr. & A. Gray ex Hook v3) and spruce (*Picea engelmannii* Parry ex Engelm. × *Picea glauca* (Moench) Voss × *Picea sitchensis* (Bong) Carrière, clone PG29 v3) transcriptomes. BLAST searches were performed using the following parameters: maximum target sequences: 500, expect threshold: 0.05, word size: 28, maximum matches in a query range: 0, gap costs: linear. Sequences retrieved from these searches were evaluated by their similarity to the Arabidopsis CSLAs in terms of amino acid sequence, total transmembrane domains, and the occurrence of the highly conserved DDDQxxRW motif (Saxena & Brown, 1997). A multiple sequence alignment of the full-length proteins from genes having these characteristics was performed using MUSCLE in MEGA-X (Kumar *et al.*, 2018). Then, a phylogenetic tree was constructed using IQ-Tree with an ultrafast bootstrap with 1000 replicates using the LG + G4 substitution model (Nguyen *et al.*, 2015). Total transmembrane domains were predicted by TMHMM server v.2.0 (Krogh *et al.*, 2001). The identification of the DDDQxxRW motif was manually completed using the multiple sequence alignment created in MEGA-X. To narrow the CSLA candidates for mannan synthesis in poplar xylem, we employed an existing RNA-seq expression database (hereafter GolS transcriptome database) generated by Unda *et al.* (2017). This expression database was derived from poplar trees expressing the Arabidopsis Galactinol Synthase (GolS3) gene that manifested in higher cellulose content and a significantly reduced lignin and mannose content compared to wild-type trees, making the dataset ideal for identifying genes that are likely involved in mannan biosynthesis.

Gene isolation from plant material

Xylem tissue from spruce (*P. engelmannii* × *glauca* × *sitchensis*, PG29; provided by the Bohlmann Lab at UBC) and poplar 717 (*P. tremula* L. × *P. alba* L., INRA 717-1B4) was used to extract RNA using the CTAB-based protocol (Kolosova *et al.*, 2004). RNA was then treated with DNase using the Turbo DNA-free kit (Life Technologies, Carlsbad, CA, USA), and subsequently exploited for the synthesis of cDNA with the iScript cDNA synthesis kit (Bio-Rad Laboratories Inc., Hercules, CA, USA).

CSLA plant expression constructs

The coding region of *PgCSLA1* (*GCHX01112248*) was amplified using BestTaq polymerase (Applied Biological Materials, Richmond, BC, Canada) and the PgCSLA1_FWD_attB and PgCSLA1_REV_attB primers (Supporting Information Table S1) carrying the Gateway attB1 and attB2 cloning sites. *PgCSLA1* was cloned into the pDONR221 (Invitrogen, Carlsbad, CA) Gateway entry vector by BP clonase recombination. *PtaCSLA1* (*Potri.008G026400*) was synthesized by Azenta (South Plainfield, NJ, USA) using the *Potri.008G026400* transcript sequence from poplar 717 as a reference (Dataset S1). The accuracy of the sequence was validated by amplifying sections of the gene from poplar 717 cDNA and sequencing. The coding

sequence of *PtaCSLA1* was cloned from the Azenta original vector, pUC-GW-Amp (Azenta), into the pDONR221 (Invitrogen, Carlsbad, CA) Gateway entry vector using the primers PtaCSLA1_FWD_attB and PtaCSLA1_REV_attB (Table S1).

Coding sequences of all candidate genes cloned into the pDONR221 plasmid were subsequently transferred into the plant expression vector pk7WG2 driven by the Arabidopsis CESA7 promoter (*AtCESA7*; Karimi *et al.*, 2002; Smith *et al.*, 2015) using LR recombination. Chemically competent *Agrobacterium tumefaciens* (strains GV3101 and EHA105) cells were transformed with each of the expression vectors carrying the putative genes following the freeze–thaw protocol (Wise *et al.*, 2006).

gRNA design

A database with all possible gRNAs targeting each of the genes of interest in poplar was created using the variant-sensitive Aspen CRISPR designer pipeline (Tsai & Xue, 2015). From this database, the gRNA1 (5′-TGGATTATGATCCGGTCGGACGG-3′) targeting the second exon of the two putative poplar *CSLA* genes (*Potri.008G026400*, *Potri.010G234100*) was selected. This gRNA contained a total of nine predicted off-targets carrying at least three mismatches in the seed region.

CRISPR-Cas9 cloning

Knockout constructs were generated by Gibson assembly following the protocol of Jacobs & Martin (2016). Briefly, the *Medicago truncatula* U6 promoter and the scaffold fragment were amplified from the pUC gRNA shuttle plasmid (Addgene plasmid #47024) using the primers SwaI.MtU6F and MtU6R and SpeI.hpR and hpF, respectively (Table S1). Then, these two fragments were cloned alongside the selected gRNA into the p201N::Cas9 plasmid (Addgene plasmid #59175) using the NEBuilder HiFi DNA Assembly Cloning Kit (New England Biolabs). Following transformation of TOP10 *Escherichia coli* (Invitrogen) competent cells with 3 µl of the Gibson reaction, PCR-positive colonies were confirmed by Sanger sequencing (Genewiz, South Plainfield, NJ, USA) of two different fragments, the first one using the primers: SpeI.hpR and gRNA1.SF.R-CSLAs, and the second one using the primers: 2X35Shyb and gRNA1.U6.F-CSLAs (Table S1). Confirmed vectors were then transferred into *A. tumefaciens* strain EHA105 for poplar transformation.

Agrobacterium-mediated transformation of Arabidopsis

Transformation of the Arabidopsis *csla 2,3,9* triple mutants was completed following the floral dip method (Clough & Bent, 1998) using the Agrobacterium GV3101 strains carrying the expression vectors. Seeds were plated on ½-strength Murashige & Skoog basal medium (MS media) (Murashige & Skoog, 1962) plates containing 50 µg ml^{-1} kanamycin, stratified at 4°C in the dark for 2 d, and subsequently germinated under constant light. Germinated seeds were transferred to soil and grown for 6 wk under long-day conditions (16 h light : 8 h dark) (Zhang *et al.*, 2006).

Genomic screening of Agrobacterium-transformed Arabidopsis plants

Genomic DNA was extracted from 7-wk-old leaf tissue from Arabidopsis complemented mutants. Leaf tissue was ground in a mortar and pestle under liquid nitrogen, and 400 µl of DNA extraction buffer containing 25 mM NaEDTA, 250 mM NaCl, 200 mM Tris HCl, and 0.5% Sodium Dodecyl Sulfate was added. Samples were centrifuged at 14 200 ***g*** for 3 min, and the supernatant was placed in a new 1.5 ml tube. DNA precipitation was achieved by adding 300 µl of isopropanol for 10 min, followed by centrifugation at 14 200 ***g*** for 5 min. The supernatant was discarded, and the pellet was washed by adding 500 µl of 70% ethanol. After centrifugation at 14 200 ***g*** for 2 min, the pellet was dried and then resuspended in sterile distilled water. Genomic screening was performed using the following gene-specific primers on the extracted DNA: PtaCSLA1_FWD and PtaCSLA1_REV, and PgCSLA1_FWD and PgCSLA1_REV (Table S1).

Arabidopsis and poplar cell wall composition

Cell wall composition was quantified using the secondary acid hydrolysis procedure (Coleman *et al.*, 2008). A modified protocol of this procedure was used to determine the total carbohydrate content of Arabidopsis stems (Glass *et al.*, 2015). Briefly, the bottom 13 cm of 7-wk-old Arabidopsis stems were collected and dried at 50°C for 48 h. For one biological replicate, seven main inflorescent stems from seven plants were pooled. Three biological replicates were obtained from each line and wild-type plants. Each pool of seven stems was ground in a 2000 Geno/Grinder® (SPEX® SamplePrep, USA) and extracted overnight with hot acetone using a Soxhlet apparatus. A total of 10 mg of extracted ground stem tissue was treated with 100 µl of 72% sulfuric acid for 5 min, then vortexed and briefly centrifuged on a bench-top centrifuge. Samples were incubated at 30°C for 1 h at 500 rpm, and then 2 ml of nanopure water was added. Next, samples were vortexed and incubated at 130°C for 75 min followed by centrifugation at 14 200 ***g*** for 5 min. Finally, the supernatant was collected and diluted (1 : 10) with nanopure water. Carbohydrate content was determined by high-performance anion exchange liquid chromatography (HPAEC) of the filtered hydrolysates. A dilution series of external standards (arabinose, rhamnose, galactose, glucose, xylose, and mannose) was used to create standard curves and determine sugar concentrations in each sample. The samples and standards were run on a Dionex Dx-600 anion-exchange HPLC (Dionex, Sunnyvale, CA) fit with a CarboPac PA1 column with distilled deionized water as an eluant at a flow rate of 0.8 ml min^{-1}. Detection was achieved with a pulsed amperometric detector fit with a gold electrode and postcolumn addition of 0.2 M sodium hydroxide at a flow of 0.5 ml min^{-1}. Meso-erythritol was used as an internal standard.

For poplar, 200 mg of 40-mesh wood powder was subjected to Soxhlet extraction. The dried samples were then treated with 3 ml of 72% sulfuric acid for 2 h with constant manual stirring

with a glass rod every 10 min. Subsequently, 112 ml of water was added, and samples were autoclaved under the same conditions described above. After autoclaving, the samples were filtered through preweighed coarse crucibles, and the remaining residues were rinsed with 150 ml of water, dried overnight at 105°C, and weighed to determine acid-insoluble lignin. The filtered aliquot was used to determine the acid-soluble lignin by measuring its UV absorbance at 205 nm. Carbohydrate content was determined by HPAEC as previously described, using fucose as an internal standard.

Alcohol insoluble residue (AIR)

Stems of 15 different transformed Arabidopsis plants were pooled together and ground to create a biological replicate for this chemical analysis. Three samples (each with the stem tissue of 15 plants) from each of the lines transformed with the *PgCSLA1* and *PtaCSLA1* genes were used to generate the AIR. For each sample, 250 mg of the ground stem tissue was ethanol extracted at 70°C for 30 min. Samples were centrifuged at 1600 ***g*** for 10 min, and the supernatant was discarded. Then, the pellet was resuspended in 2 ml of chloroform : methanol (3 : 2 v/v) solution and mixed at room temperature overnight. Samples were centrifuged at 1600 ***g*** for 10 min, and the supernatant was discarded. The pellet was resuspended again in 2 ml of chloroform : methanol (3 : 2 v/v) solution and mixed at room temperature for 1 h. The samples were again centrifuged at 1600 ***g*** for 10 min, and the supernatant was discarded. Subsequently, the pellet was washed in 100% ethanol and centrifuged at 1600 ***g*** for 10 min. Then, the pellet was washed with 65% ethanol, centrifuged at 1600 ***g*** for 10 min, and resuspended in 80% ethanol and centrifuged at 1600 ***g*** for 10 min again. Finally, the pellet was washed with 100% ethanol, centrifuged at 1600 ***g*** for 10 min, and dried overnight in an oven at 45°C.

Mannan-rich extract preparation and linkage analysis

A mannan-rich extract from WT, *csla 2,3,9* triple mutant, and *csla 2,3,9 PgCSLA1*-complemented Arabidopsis lines was isolated according to Pattathil *et al.* (2012). This protocol used 200 mg of AIR extracted tissue from each genotype. AIR tissue was subjected to sequential extractions using 50 mM ammonium oxalate (pH 5.0), 50 mM sodium carbonate with 0.5% sodium borohydride, 1 M KOH with 1.0% sodium borohydride, and 4 M KOH with 1.0% sodium borohydride. Each step involved 24 h incubation with gentle shaking (100 rpm), centrifugation at 3900 ***g*** for 15 min, and supernatant collection at 4°C. The final 4 M KOH extract was dialyzed using 3500 Da molecular weight tubing (S632724; Spectrum Laboratories Inc., CA, USA) and then lyophilized for 2 d. Once dried, this extract was used for linkage analysis.

Linkage analysis was performed following the protocol of Black *et al.* (2021). Briefly, 400 µg of lyophilized extract was resuspended in 400 µl of dry DMSO for 2 d. To this, 400 µl of NaOH/DMSO was added and stirred for 20 min. After which, 100 µl of iodomethane was added and gently stirred for 40 min, and then an additional 100 µl iodomethane was added to ensure complete methylation. Next, 2 µl of water was added, and the iodomethane was evaporated under a stream of nitrogen. The sample was extracted with 2 ml of DCM (dichloromethane), vortexed for 20 s, and separated by low-speed centrifugation. The aqueous layer was discarded and the DCM layer was washed five times with water before being transferred to a new tube and dried under a stream of nitrogen. For hydrolysis, 200 µl of 2 M TFA and 20 µl of inositol (1 mg ml^{-1}) were added, and the sample was incubated at 120°C for 2 h. After cooling, the sample was dried under a stream of nitrogen, treated with 100 µl of isopropanol, and evaporated. This step was then repeated. For reduction, 300 µl of 10 mg ml^{-1} sodium borodeuteride in 1 M ammonium hydroxide was added and incubated overnight at room temperature. The sample was neutralized with five drops each of glacial acetic acid and methanol, and then dried under a stream of nitrogen. A 9 : 1 methanol : acetic acid solution (100 µl) was added and evaporated, and this was repeated three times until a white residue formed. The samples were acetylated by adding 250 µl of acetic anhydride and 230 µl of concentrated TFA, and then permitted to incubate at 50°C for 20 min. After cooling, 1 ml of isopropanol was added, and the sample was dried under a stream of nitrogen; this was then repeated to remove TFA. The sample was washed with 2 ml of water and DCM, vortexed, and centrifuged at 1200 ***g*** for 5 min. Then, the aqueous layer was discarded, and after four washes with water, the organic DCM layer was transferred to a new tube, dried under a stream of nitrogen, diluted in 150 µl of DCM, and transferred to a brown glass GC tube. GC-MS analysis of the partially methylated alditol acetates was performed using an Agilent 7890A GC equipped with a TQ8030 MSD. Separation was achieved on a Supelco SP-2330 fused silica capillary column (30 m × 0.25 mm ID) under the following conditions: 60°C for 1 min, ramped at 27.5°C min^{-1} to 170°C, then at 4°C min^{-1} to 235°C (held for 2 min), followed by 3°C min^{-1} to a final temperature of 240°C (held for 12 min). A commercial glucomannan extract was used to determine linkage elution times, and identities were confirmed by ion profile comparison with the Complex Carbohydrate Research Center spectral database for partially methylated alditol acetates.

Preparation of soluble hemicelluloses and PACE analysis

Preparation of soluble hemicelluloses and a carbohydrate gel electrophoresis (PACE) analysis was carried out following the protocol of Goubet *et al.* (2002). Briefly, 20 mg of AIR were treated with 1 ml of 4 M potassium hydroxide at room temperature for 1 h and then centrifuged at 1400 ***g*** for 5 min. The supernatant was loaded onto a PD-10 desalting column (GE Healthcare, IL, USA) and eluted with 50 mM ammonium acetate (pH 6.0). The eluted hemicelluloses were digested overnight with 2 µl of *Cellvibrio japonicus* Man26A (*Cj*Man26A) mannanase (University of Newcastle) or *Aspergillus nidulans* GH5 (*An*GH5) mannanase (Novozymes) in 50 mM ammonium acetate (pH = 6.0) at 37°C. For sequential digestions, 2 µl of β-glucosidase (β-Glc), β-mannosidase (β-Man), and α-galactosidase (α-Gal) enzymes were

added after the initial digestion with either *Cj*Man26A or *An*GH5. Enzymes were deactivated after digestion by heat treatment at 100°C for 20 min. Samples were then derivatized with 8-aminonaphthalene-1,3,6-trisulfonic acid overnight and dried at 60°C in a speedvac (Thermo Fisher Scientific, Waltham, MA, USA). Samples were then resuspended in 100 µl of 3 M urea, and 2 µl was loaded onto a 20% acrylamide resolving gel. The electrophoresis was carried out at 200 V for 30 min and then 1000 V for 120 min.

Agrobacterium-mediated transformation of poplar

Poplar leaf discs were transformed following the protocol of Wilkerson *et al.* (2014). Briefly, discs were cut from 5-wk-old poplar 717 leaves and cocultivated for 1 h at 28°C with each of the *A. tumefaciens* strains (EHA105; OD_{600nm} = 0.1–0.2) transformed with the expression vectors. Leaf discs were placed abaxial-side-up on WPM media (0.1 µM NAA, 0.1 µM BA, and 0.1 µM TDZ) and incubated in the dark for 2 d. Then, leaf discs were transferred to WPM media (0.1 µM NAA, 0.1 µM BA, and 0.1 µM TDZ) containing 250 $\mu g \cdot ml^{-1}$ cefotaxime and 500 $\mu g \cdot ml^{-1}$ carbenicillin to eliminate *A. tumefaciens*, and maintained in darkness for 2 d. Afterward, leaf discs were placed on WPM (0.1 µM NAA, 0.1 µM BA, and 0.1 µM TDZ) selection media containing 50 $\mu g \cdot ml^{-1}$ of kanamycin for 5 wk. Next, leaf discs were transferred to WPM shooting media (0.01 µM BA, 250 $\mu g \cdot ml^{-1}$ cefotaxime, 500 $\mu g \cdot ml^{-1}$ carbenicillin, and 50 $\mu g \cdot ml^{-1}$ kanamycin) for 4 wk and subsequently moved to WPM rooting media (0.01 µM NAA, 250 $\mu g \cdot ml^{-1}$ cefotaxime, 500 $\mu g \cdot ml^{-1}$ carbenicillin, and 50 $\mu g \cdot ml^{-1}$ kanamycin). After 5 wk of growth, plants were genomically screened using the gene-specific primers (Table S1), and positive transformants were propagated in antibiotic-free WPM media (0.01 µM NAA). Apical stem pieces from propagated transformants (eight biological replicates per line) were grown for 4 wk, and then the subsequently rooted plantlets were transferred to the soil. This protocol was concomitantly followed using wild-type poplar 717 leaf discs as a control, with the exception that all media were antibiotics-free.

Genomic screening of poplar

Genomic DNA was extracted from leaves of wild-type and transformed poplar in tissue culture following the same procedure employed with Arabidopsis. The target genes were detected from the genomic DNA by using gene-specific primers for *PtaCSLA1* and *PgCSLA1* (Table S1). In the case of the poplar lines transformed with the p201NCas9::gRNA1 construct, the genomic screening targeted the *Cas9* gene using the Cas9_p59175_FWD and Cas9_p59175_REV primers (Table S1). For these trees, only positive lines were subsequently analyzed by Sanger sequencing to confirm the mutations.

Gene expression analysis of spruce CSLAs in poplar

Total RNA was isolated from poplar xylem scrapings using the PureLinkTM RNA Mini Kit (Invitrogen). RNA was treated with DNase using the Turbo DNA-free kit (Ambion, Life Technologies, Carlsbad, CA, USA) and then used to synthesize cDNA with the iScript cDNA Synthesis Kit (Bio-Rad Laboratories). Relative expression levels of *PgCSLA1* (*GCHX01112248*; primers qPCR_PgCSLA1_FWD and qPCR_PgCSLA1_REV) were quantified using BlasTaq 2× quantitative polymerase chain reaction (qPCR) MasterMix (Applied Biological Materials, Richmond, BC, Canada) (Table S1). PCR reactions consisted of 5 µl BlasTaq 2× master mix, 0.3 µl of reverse and forward primers (10 µM), 1 µl cDNA, and deionized water to a volume of 10 µl. Three technical replicates were used per sample. qPCR parameters were as follows: 5 min at 95°C, 39 cycles of 95°C for 5 s, and 60°C for 30 s, then 1 cycle of 94°C for 10 s, followed by a melt curve cycle of 56°C to 95°C at 0.5°C increments for 5 s. Average expression of the reference gene *PtrEF1β* (*Potri.009G018600*; primers PtEF1β-qPCR-FWD and PtEF1β-qPCR-REV) was used to calculate the relative expression of the target genes (Table S1). Fold change was calculated relative to the lowest-expression line by subtracting the normalized expression from the highest reported target gene.

Determination of mutant spectrums in CRISPR poplar lines

Using genomic DNA isolated from lines that proved positive after the genomic screening of *Cas9*, a PCR was performed using the primers CRISPR_PtaCSLA1_FWD and CRISPR_PtaCSLA1_REV to amplify the *PtaCSLA1* sequence, and CRISPR_PtaCSLA2_FWD and CRISPR_PtaCSLA2_REV to amplify the *PtaCSLA2* (Table S1). PCR products were Sanger sequenced using the same primers employed for amplification and analyzed for possible mutations via TIDE (Brinkman *et al.*, 2014). Confirmation of a biallelic or monoallelic mutation of each gene was completed by analyzing the chromatograms and comparing them with the known gene sequences of each possible allele.

Poplar growth conditions and measurement

The apical meristems of 6-wk-old transformed plants and corresponding controls were transferred to two-gallon pots containing perennial soil mix (50% peat, 25% fine bark, and 25% pumice; pH 6.0). Trees were grown on flooding tables under 16 h of light at the UBC glasshouse for 5 months. At the time of harvest, stem height, stem diameter, and weight of fresh biomass were recorded. Height was measured from root collar to tree apex, whereas diameter was measured 10 cm above root collar with digital calipers. The weight of fresh biomass was recorded using the whole tree cut 10 cm above the root collar. Developing xylem was collected by scraping the debarked stems and subsequently flash-frozen in liquid nitrogen and stored at −80°C. Stems were air-dried for 2 wk, and then a 10-cm piece originating from the base of the cut stem was ground using a Wiley mill to pass a 40-mesh sieve.

Poplar cross-section staining

Wood samples from 5-month-old transgenic poplar and control trees were soaked overnight in dH_2O. Samples were then cut into

40 µm cross-sections with a Spencer AO860 hand sliding microtome (Spencer Lens Co., Buffalo, NY, USA) and stored in falcon tubes with dH_2O. Samples were treated with 0.1% Pontamine Fast Scarlet 4B for 10 min and then washed twice with TBST (Tris Buffered Saline; 10 mM Tris-buffer, 0.25 M NaCl, pH 7, with 0.1% Tween). Then, the sections were mounted onto glass slides and visualized on an Olympus FV1000 MPE laser scanning microscope (Olympus Corp., Tokyo, Japan) employing Olympus Fluoview software (FV10-ASW2).

Mannan antibody detection

The prepared cross-section samples described above were also subjected to antibody labeling. Briefly, immunolabeling was performed as follows: wood cross-sections were treated with 1 M KOH solution for 1 h, washed with TBST, and then blocked with 5% BSA in TBST for 90 min at room temperature. Then, sections were incubated overnight with diluted (1 : 20) Rat LM21 anti-(1,4)-β-mannan primary antibody (Kerafast, US) and Mouse CCRC-M138 antixylan primary antibody (Carbosource) in the blocking solution at 4°C, and subsequently washed twice with TBST for 5 min. Next, samples were treated with diluted (1 : 400) Goat anti-Rat IgG Alexa Fluor™ 568 and diluted (1 : 1000) Goat anti-Mouse IgG Alexa Fluor™ 488 secondary antibodies (Invitrogen) in the blocking solution and incubated for 1 h at room temperature. Samples were washed three times with TBST and mounted on glass slides for visualization using an Olympus FV1000 MPE laser scanning microscope (Olympus Corp.) using the Olympus Fluoview software (FV10-ASW2).

Saccharification assay

Pretreatment and saccharification assays were performed as previously described (Van Acker *et al.*, 2013), with minor modifications. Samples of ground, dry xylem powder (15 mg) were subjected to either no pretreatment or acid pretreatment, with two technical replicates per treatment. Briefly, samples subjected to mild acid pretreatment were incubated in 2% sulfuric acid at 80°C for 2 h. After incubation, the samples were neutralized and washed four times with water. The aliquots for saccharification without pretreatment were similarly washed four times with water. Both sets of samples were dried for 4 d at 50°C. Then, 1 ml of 0.1 M acetic acid buffer solution (pH 4.8) was added to the washed wash the samples and incubated at 50°C, shaking at 300 rpm. Cellic CTec3 (Novozymes, Bagsværd, Denmark) enzyme was diluted 100 times, and 100 µl was added to each sample. After 4, 24, 48, and 72 h, 20 µl of aliquots were taken from the saccharification sample and diluted before HPAEC quantification. The concentration of glucose and xylose in the timepoint samples was determined by Dx-600 anion-exchange HPLC (Dionex, Sunnyvale, CA, USA) as described above.

Statistical analysis

Square-root or natural-log transformations were used on data to meet model assumptions of normality and homoscedasticity. When met, the means of more than two groups were compared using a one-way ANOVA. If the ANOVA showed a significant difference, a Tukey HSD *post hoc* analysis with a Bonferroni correction was conducted to identify the significant pairs. Data where the assumptions were not met were evaluated with a non-parametric test, using a Kruskal–Wallis test followed by a Dunn's *post hoc* analysis also employing a Bonferroni correction. The statistical significance of the *P*-values was assessed with an experimentwise error rate of 0.05. All analyses were conducted in the R Software Environment (v.4.3.1).

Results

Bioinformatics of putative CSLAs

In poplar, we confirmed that five genes are predicted to be putative CSLA candidates: *Potri.008G026400*, *Potri.010G234100*, *Potri.006G116900*, *Potri.009G149700*, and *Potri.004G1890* (Fig. 2; Liepman *et al.*, 2005; Suzuki *et al.*, 2006). By contrast, for spruce we identified only one gene as a likely candidate: *GCHX01112248* (Fig. 2). These putative CSLAs displayed similar characteristics to known Arabidopsis CSLAs in terms of their amino acid sequence, the number of transmembrane domains (Table S2), and the presence of the conserved DDDQxxRW motif (Fig. S1). To narrow the CSLA candidates for mannan synthesis in poplar xylem, we used as a reference the transcriptome database generated by Unda *et al.* (2017) that clearly showed a distinct repression in the transcript abundance of two of the five putative poplar genes in trees that had a significant reduction in mannan content (see Materials and Methods section). Specifically, *Potri.008G026400* (hereafter *PtaCSLA1*) and *Potri.010G234100* (hereafter *PtaCSLA2*) were differentially expressed in the poplar xylem of the GolS transgenic trees (Unda *et al.*, 2017), with *PtaCSLA1* being the highest expressed putative CSLA in wild-type trees as well as the most significantly downregulated gene in the transgenic trees (Table S3). Hence, *PtaCSLA1* and *GCHX01112248* (hereafter *PgCSLA1*) were selected to be functionally evaluated in the Arabidopsis triple mutant *csla2,3,9*.

CSLAs from spruce and poplar increase mannose content in the Arabidopsis *csla2,3,9* triple mutant

The Arabidopsis *csla2,3,9* triple mutants were transformed with the *AtCESA7::PtaCSLA1* and *AtCESA7::PgCSLA1* constructs via *Agrobacterium*-mediated transformation, and multiple lines carrying the *AtCESA7::PtaCSLA1* and *AtCESA7::PgCSLA1* constructs were generated. Each line was confirmed by genomic screening using leaf tissue and gene-specific primers (Table S1). The complemented lines grew similarly to the wild-type and *csla2,3,9* mutant Arabidopsis plants, whereby no changes in the overall growth or developmental timing were observed. To determine if the complemented lines recovered the phenotype of the *csla2,3,9* mutants depleted of mannan, a polysaccharide compositional analysis was performed using the bottom sections of 7-wk-old stems of two positive

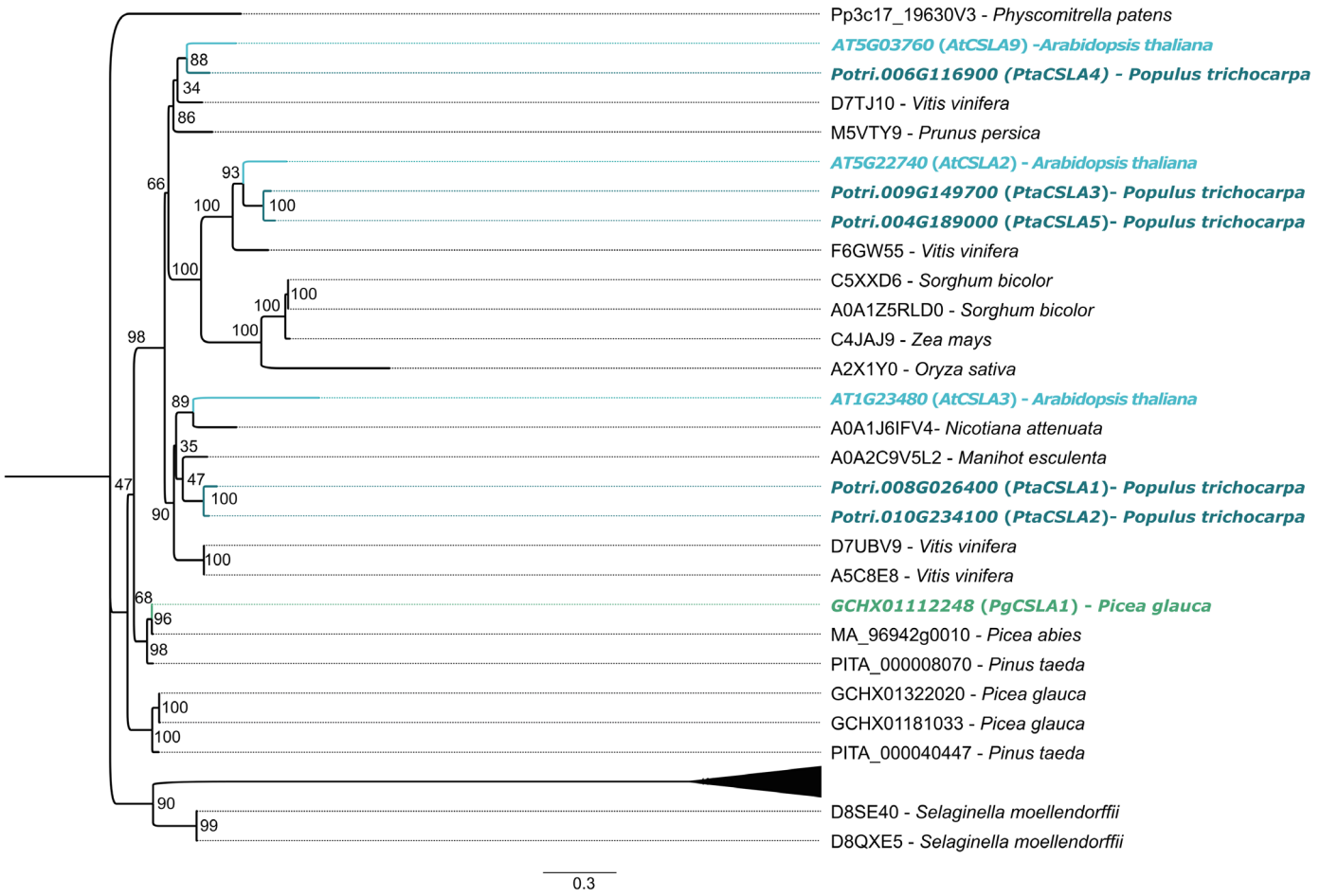

Fig. 2 Phylogenetic tree of putative poplar and spruce Cellulose Synthase-Like A (CSLA) orthologues. CSLAs from Arabidopsis are marked in cyan colour (*AT5G22740*: *AtCSLA2*; *AT1G23480*: *AtCSLA3*; *AT5G03760*: *AtCSLA9*). Poplar candidates are in teal, and the Spruce PG29 candidate gene selected for the functional analysis in Arabidopsis is in light green. Numbers in the labels of the nodes correspond to the UFBoot support. The scale at the bottom shows phylogenetic distance of the associations. The tree was constructed using the LG + G4 substitution model.

transgenic lines for each gene, wild-type, and the triple mutant plants. It was apparent that the triple mutants were complemented by both constructs, *AtCESA7::PtaCSLA1* and *AtCESA7::PgCSLA1*, as the mannose content increased relative to the triple mutant plants. In two of the lines carrying the *AtCESA7::PtaCSLA1* construct, mannose content reached 22.39 μg mg^{-1} of extracted tissue (Fig. 3; Table S4) relative to 22.45 μg mg^{-1} found in the corresponding wild-type control plants, while in the lines complemented with the *AtCESA7::PgCSLA1* construct, the recovered mannose content was as much as 25.79 μg mg^{-1} relative to the 23.83 μg mg^{-1} found in the corresponding wild-type control plants (Fig. 3; Table S5). In both experiments, no mannose was detected in the *csla2,3,9* triple mutant, as previously described (Goubet *et al.*, 2009). No major significant changes in other cell wall compositional sugars were observed between the complemented lines and the wild-type plants (Tables S4, S5). Together, these results suggest that both *PtaCSLA1* and *PgCSLA1* encode functional mannan synthases capable of producing mannan in the secondary cell walls of Arabidopsis.

PgCSLA1 recovers 4-Man linkage content in the Arabidopsis *csla2,3,9* triple mutant

To corroborate the production of mannan in the *PgCSLA1*-complemented lines and the nature of the linkages formed, we performed a methylation analysis using stem tissue from wild-type plants, *csla2,3,9* mutants, and *csla2,3,9*-complemented plants. Using this tissue, we conducted a series of sequential extractions following the protocol described by Pattathil *et al.* (2012) to isolate a mannan-rich extract. This mannan-rich extract was subsequently used for linkage analysis, employing a commercially available glucomannan extract to determine the elution time and ion profile of the linkages of interest (4-Man and 4-Glc). We showed that elution times of 19.54 and 20.52 min represent 4-Man and 4-Glc, respectively (Fig. S2). We also confirmed that *m/z* 118 and *m/z* 233 are the diagnostic ions for both 4-Man and 4-Glc linkages using the Complex Carbohydrate Research Center spectral database for partially methylated alditol acetates. Using this information, we demonstrated that 4-Man was only present in wild-type and *PgCSLA1*-

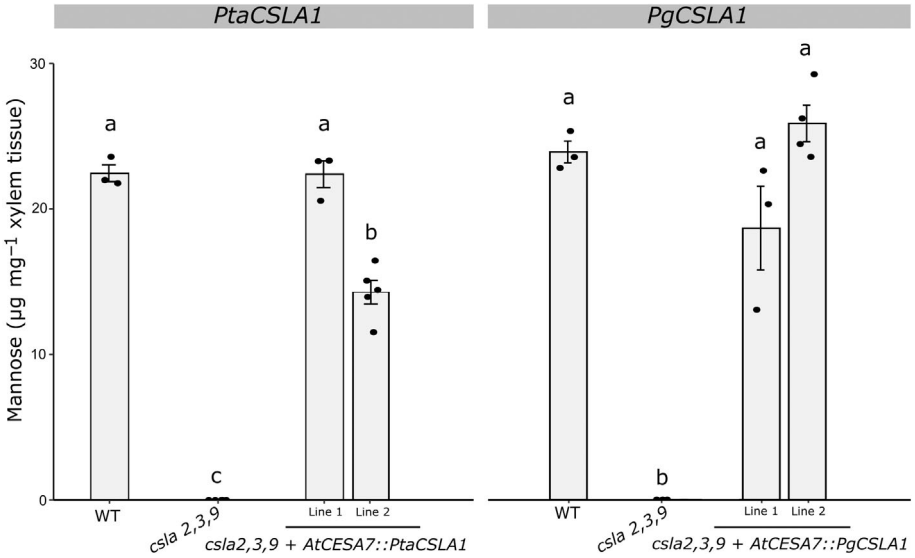

Fig. 3 Mannose composition of Arabidopsis wild-type plants, *csla2,3,9* triple mutants, and *csla2,3,9* mutants complemented with *AtCESA7::PtaCSLA1* and *AtCESA7::PgCSLA1*. Independent whole-cell wall analyses (micro-Klasons) were performed to evaluate the mannose content in the complemented mutant lines expressing *PtaCSLA1* and *PgCSLA1*. Mutant lines complemented with either the putative poplar (*PtaCSLA1*) or spruce (*PgCSLA1*) CSLA exhibited a significantly higher mannose content in Arabidopsis stems compared to non-complemented mutants (Kruskal–Wallis and *post hoc* analysis, P-value < 0.05, n = 3–4 for each line, different letters indicate significant differences). Error bars indicate the SE. Values are represented in µg mg^{-1} of extracted tissue. CSLA, Cellulose Synthase-Like A; WT, wild-type Col-0 Arabidopsis.

complemented lines, whereas it was absent in the *csla2,3,9* mutants (Fig. S2). In general, our results support that mannan containing 4-Man linkages is being produced in the *PgCSLA1*-complemented lines, contrary to what occurs in the *csla2,3,9* mutants depleted of mannan.

PtaCSLA1 and PgCSLA1 produce a random patterned glucomannan in Arabidopsis *csla2,3,9* triple mutant

In Arabidopsis, CSLA2 and CSLA9 synthesize glucomannan with inherently different backbone structures. CSLA2 produces a patterned glucomannan, in which glucose and mannose residues follow a specific repeating sequence (Yu *et al.*, 2022). By contrast, CSLA9 generates glucomannan with a non-patterned backbone, where these residues are distributed more randomly (Yu *et al.*, 2022). The potential for galactosyl side-chain decoration depends on both the backbone pattern and the presence of specific mannan galactosyltransferases (Yoshimi *et al.*, 2025). Depending on this combination, the resulting polysaccharide may or may not be decorated with galactose residues (Yu *et al.*, 2022). The degree of galactosylation highly influences mannan properties and plays an important role in mannan-cellulose interactions (Voiniciuc *et al.*, 2019; Yoshimi *et al.*, 2025). We performed PACE analysis to characterize the type of mannan that both PtaCSLA1 and PgCSLA1 were producing in the complemented *csla2,3,9* Arabidopsis lines. Two enzymes were employed for this analysis, *Cj*Man26A and *An*GH5 β-mannanases. The former cleaves β-Man-(1,4)-β-Glc bonds, but does not cleave β-Glc-(1,4)-β-Man; this enzyme cannot tolerate Gal or acetate substitutions at the −1 position. By contrast, *An*GH5 cleaves β-Man-(1,4)-β-Glc and does not digest β-Glc-(1,4)-β-Man bonds; however, it tolerates single Gal substitutions at the −1 position. In addition, sequential digestions were completed using β-glucosidase (β-Glc), β-mannosidase (β-Man), and α-galactosidase (α-Gal). The main oligosaccharides released after treating wild-type and *PtaCSLA1* complemented lines samples with *Cj*Man26A corresponded to M, MM, GMM, and MGMM (Fig. 4a), which is consistent with the patterns previously observed in the Arabidopsis *csla2* single mutant, where mannan production depends on CSLA9 activity and the oligosaccharides liberated have a high degree of polymerization. In the *csla2,3,9* triple mutant, no detectable oligosaccharides were apparent. When treating the *Cj*Man26A digested sample with β-Glc and β-Man, all oligosaccharides were converted into mono- and disaccharides (Fig. 4b).

Similar results were observed in *csla2,3,9* Arabidopsis *Pg*CSLA1 complemented lines digested with *Cj*Man26A (Fig. 5a, b). To confirm these results, we treated the complemented lines with *An*GH5 and subsequently with β-Glc, β-Man, and α-Gal. Similar to the *Cj*Man26A digestion, it was observed that all oligosaccharides were converted to either G, M, or MM (Figs S3, S4). In general, our results are similar to those observed in the *csla2* Arabidopsis mutant, where CSLA9-dependent oligosaccharides are formed, indicating that *PtaCSLA1* and *PgCSLA1* synthesize a non-patterned glucomannan absent of galactosyl side chains.

Generation of double and single knockout CSLA poplar lines

To confirm the activity of the putative poplar CSLA genes functionally evaluated in the Arabidopsis *csla2,3,9* triple mutants and to further understand the role of mannan in cell wall integrity, hybrid poplar trees were transformed with a CRISPR-Cas9 construct carrying the gRNA1 (3′-TGGATTATGATCCGGTC GGA-5′). This gRNA targeted a conserved region in exon two of the CSLA poplar candidate genes and was designed such that the target region was SNP-free. After tree regeneration, PCR was employed to confirm the presence of the *Cas9* gene in tissue culture trees, and positive lines were sent for Sanger sequencing. During the plant regeneration process, we observed that multiple trees were able to grow on the selection media; however, most of them were not positive when *Cas9* was amplified, nor did they carry a mutation in the target sequence.

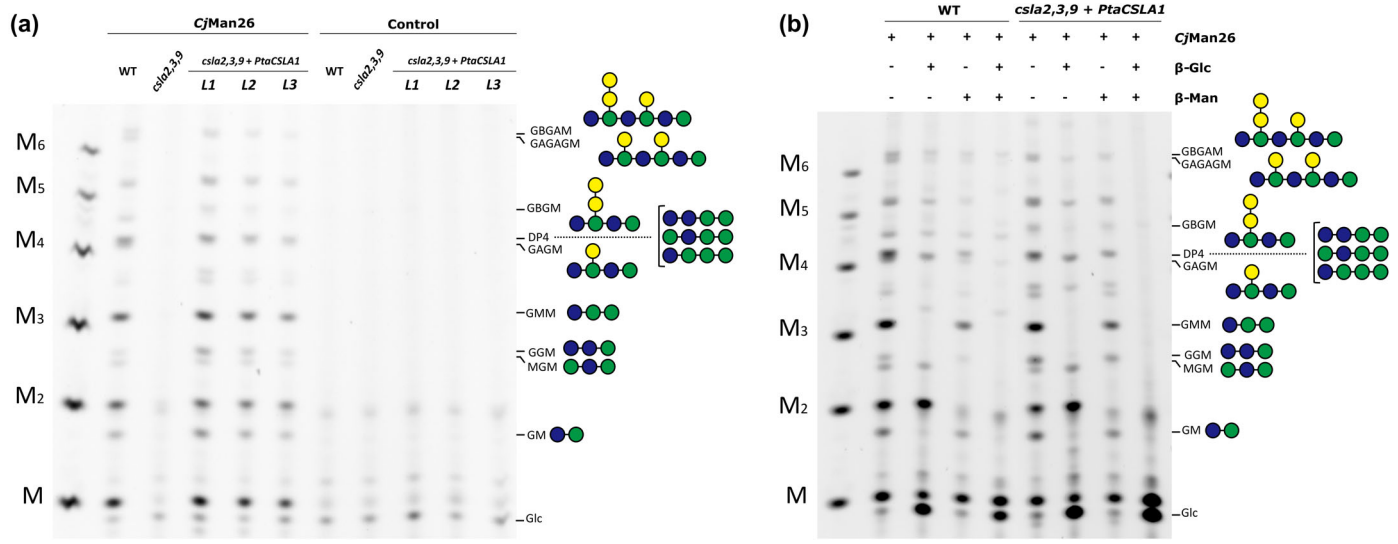

Fig. 4 Mannan backbone structure in *csla2,3,9 PtaCSLA1-complemented* lines digested with *Cj*Man26A. (a) Arabidopsis stem material from three different complemented lines (L1, L2, and L3) with *PtaCSLA1* was analyzed by PACE. Hemicelluloses were extracted from wild-type plants, the *csla2,3,9* triple mutants, and complemented lines using alkali before being hydrolyzed with *Cj*Man26A. The products were derivatized with 8-amino-naphthalene-1,3,6-trisulfonic acid and separated by PACE gel electrophoresis. The three complemented lines yielded oligosaccharides with a high degree of polymerization, showing a similar pattern to that of Arabidopsis *csla2* mutants. (b) Characterization of *Cj*Man26A-digested products by PACE using β-glucosidase (β-Glc) and β-mannosidase (β-Man) enzymes. Most of the oligosaccharides are reduced to mono- and disaccharides in the complemented line (only Line 1 is shown), suggesting that the mannan synthesized by PtaCSLA1 lacks a discernible pattern and remains undecorated with Gal residues. Mannan oligosaccharide standards M to M6. Green circles: mannose residues, blue circles: glucose residues, yellow circles: galactose residues. M, Man; G, Glc; DP, Degree of polymerization.

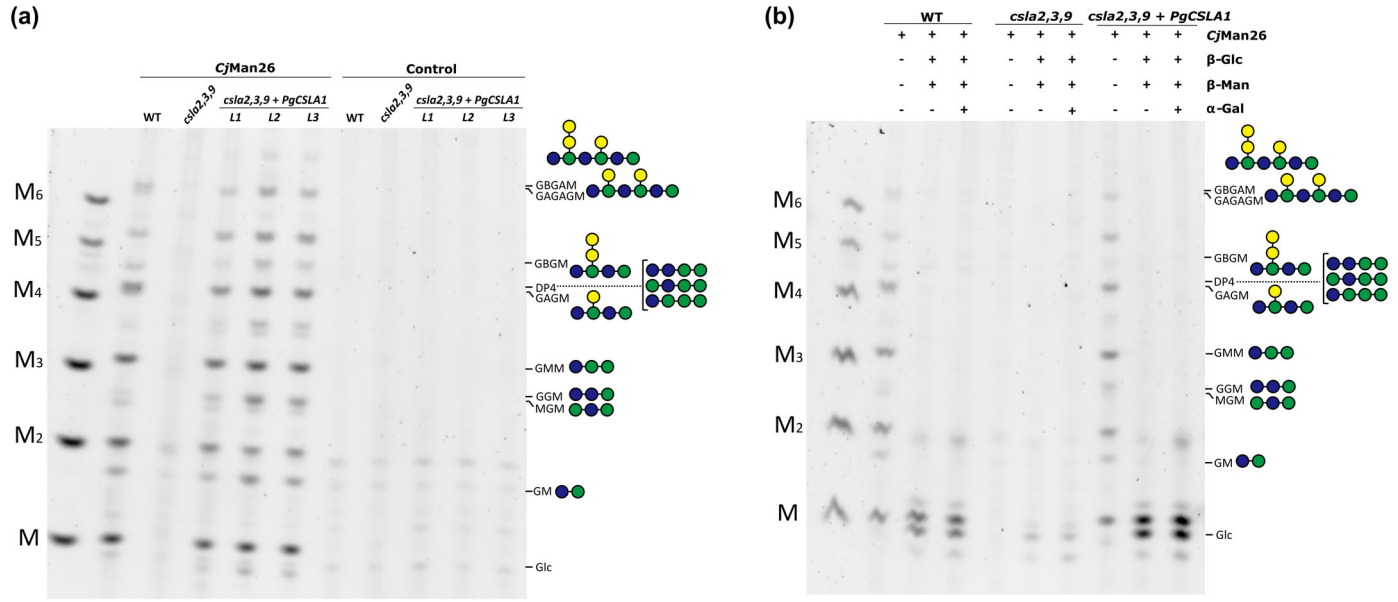

Fig. 5 Mannan backbone structure in *csla2,3,9 PgCSLA1-complemented* lines digested with *Cj*Man26A. (a) Arabidopsis stem material from three different complemented lines (L1, L2, and L3) with *PgCSLA1* was analyzed by preparation of soluble hemicelluloses and carbohydrate gel electrophoresis (PACE). Hemicelluloses were extracted from wild-type plants, the *csla2,3,9* triple mutants, and complemented lines using alkali before being hydrolyzed with *Cj*Man26A. The products were derivatized with 8-amino-naphthalene-1,3,6-trisulfonic acid and separated by PACE gel electrophoresis. The three complemented lines yielded oligosaccharides with a high degree of polymerization, showing a similar pattern to that of Arabidopsis *csla2* mutants. (b) Characterization of *Cj*Man26A digested products by PACE using α-galactosidase (α-Gal), β-glucosidase (β-Glc), and β-mannosidase (β-Man) enzymes. Most of the oligosaccharides are reduced to mono- and disaccharides in the complemented line (only Line 1 is shown), suggesting that the mannan synthesized by PgCSLA1 lacks a discernible pattern and remains undecorated with Gal residues. Mannan oligosaccharide standards M to M6. Green circles: mannose residues, blue circles: glucose residues, yellow circles: galactose residues. M, Man; G, Glc; DP, Degree of polymerization.

Multiple lines with indels in *Potri.008G026400* and *Potri.010G234100* (hereafter *PtaCSLA1/2* KO lines) were obtained according to the results from Sanger sequencing. One line with a unique mutation in *Potri.008G026400* (hereafter *PtaCSLA1* KO) was also generated. These lines contained biallelic frameshift mutations in the target genes, and the indels were either a single nucleotide insertion or deletion relatively close to the PAM region (Fig. S5a,b). Lines where the *Cas9* gene was confirmed positive had a 100% success rate of mutation for at least one of the targeted genes. A summary of the mutations detected in three *PtaCSLA1/2* KO lines and the *PtaCSLA1* KO line is found in Table S6. These poplar lines were clonally propagated and transferred to soil and grown in the glasshouse.

Mutation of CSLAs in hybrid poplar does not affect plant growth

Both wild-type and knockout lines were grown and harvested after 5 months of growth in a glasshouse. In general, no substantial alterations in height, diameter, and fresh biomass were detected in the transformed lines compared to the wild-type trees grown under the same conditions, at the same time in the glasshouse (Table S7).

Poplar CSLA knockouts exhibit changes in mannan cell wall content

The xylem cell wall chemical composition of the transformed lines was ascertained by performing a whole cell wall analysis (Klason). An examination of the individual carbohydrates by HPAEC revealed that in both the *PtaCSLA1* single and *PtaCSLA1/2* double knockouts, mannose was absent (Fig. 6). No significant differences were observed in the content of other structural sugars when the mutated lines were compared to the wild-type control (Table 1).

In addition, immunofluorescence labeling of mannan polysaccharides was performed on stem sections of the knockouts and wild-type control trees using the LM21 antibody. As shown in Fig. 7, mannan labeling intensity was absent in both single and double knockouts compared to the wild-type control, but xylan and cellulose remained similar. Mannose content, determined by HPAEC, and mannan intensity observed during immunolabeling were indistinguishable between single and double knockout lines. Regarding lignin content, we did not observe statistically significant differences; however, in the single and double knockout lines, total lignin increased slightly from 20.602% up to 21.979% total cell wall content (Table S7). Together, these results confirm that *PtaCSLA1* is indeed involved in mannan synthesis in poplar trees and imply it is the most significant contributor to the synthesis of mannan in the secondary cell walls of poplar.

Ectopic expression of PgCSLA1 in poplar does not lead to a yield penalty

Following the results obtained after complementation of the Arabidopsis *csla2,3,9* triple mutant with the *AtCESA7::PgCSLA1* construct, we transformed poplar 717 with the same functional construct using *Agrobacterium*, as previously described. A total of five positive transgenic lines were selected for further analysis. Reverse transcription-qPCR was used to measure the transgene expression in developing xylem tissue and revealed that there was variation in expression and that line 3 had the highest transcript abundance (Fig. S6). Positive lines were transferred to the glasshouse to grow in soil for 5 months. After this time, trees were harvested, and growth parameters were measured. The transgenic lines did not display significant differences in stem diameter, height, and biomass compared to the wild-type trees (Table S8).

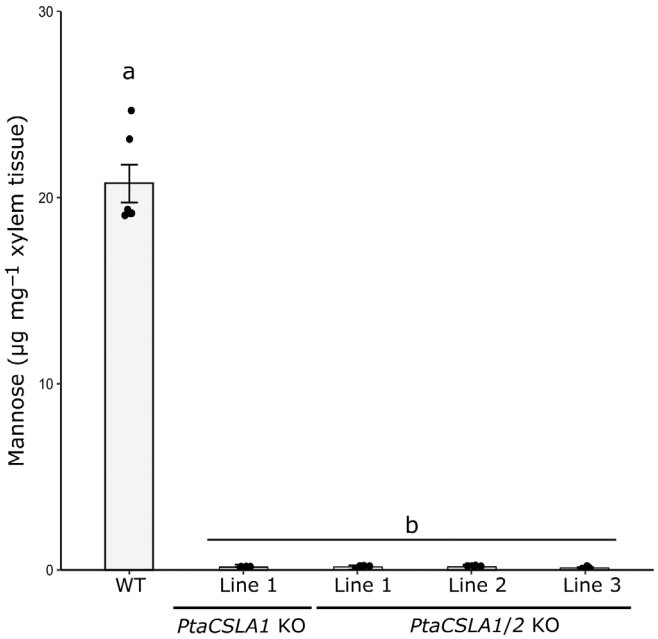

Fig. 6 Mannose composition from wild-type poplar trees and single and double Cellulose Synthase-Like A (CSLA) poplar knockouts. A Kruskal–Wallis and *post hoc* analysis was used to evaluate differences in mannan content in the wild-type trees and the knockout lines (P-value < 0.05, n = 5–6 per line, different letters indicate significant differences). All knockout lines showed a significant reduction in the amount of mannose in the xylem. Error bars indicate the SE. KO, knockout; WT, wild-type poplar 717.

PgCSLA1 expression increases mannan content in poplar stems

To investigate the impact of ectopic expression of *PgCSLA1* on poplar cell wall composition, a total cell wall composition analysis was again performed using the extract-free xylem tissue of wild-type and five of the transgenic poplar lines generated. No significant differences were noted in acid-insoluble, acid-soluble, or total lignin content when comparing the transgenic lines to the wild-type controls (Table S8). Four lines showed higher amounts of mannose compared to the wild-type trees; however, only line 3 (P-value < 0.001) and line 5 (P-value = 0.0012) were statistically significantly different (Fig. 8). These two lines showed an increase of up to 11.6% in mannan content compared to the wild-type trees; in these lines, mannose content was found

Table 1 Structural cell wall carbohydrates in the xylem of single and double Cellulose Synthase-Like A (CSLA) poplar knockouts.

Genotype	Ara	Rha	Gal	Glc	Xyl
WT	2.08 (0.23)	2.89 (0.18)	6.54 (0.36)	446.90 (3.07)	176.93 (2.76)
PtaCSLA1 KO Line 1	1.83 (0.21)	3.15 (0.24)	6.68 (0.27)	451.27 (3.75)	182.36 (5.80)
PtaCSLA1/2 KO Line 1	3.15 (0.28)	3.87 (0.21)	8.55 (0.24)	438.75 (4.53)	185.22 (1.62)
PtaCSLA1/2 KO Line 2	2.77 (0.21)	3.75 (0.12)	7.79 (0.53)	435.66 (3.25)	186.41 (1.64)
PtaCSLA1/2 KO Line 3	2.05 (0.35)	3.09 (0.38)	6.60 (0.64)	448.20 (6.56)	180.70 (5.96)

Values represent μg mg^{-1} of extract-free xylem tissue across five biological replicates per line. One-way ANOVA with a Tukey *post hoc* test was used to evaluate statistical differences among structural sugars besides mannose, including arabinose (Ara), rhamnose (Rha), galactose (Gal), glucose (Glc), and xylose (Xyl) (P-value < 0.05, n = 5–6 per line). No significant differences were detected for these structural sugars. The SE is represented in brackets. KO, knockout; WT, wild-type poplar 717.

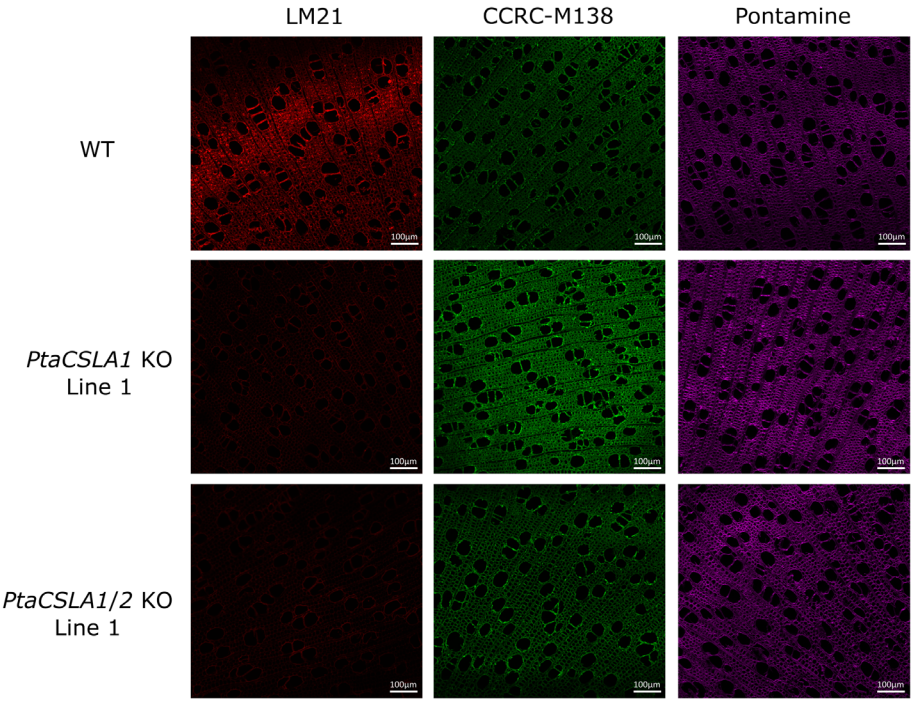

Fig. 7 Immunofluorescence labeling of xylem tissue from wild-type poplar trees, single, and double Cellulose Synthase-Like A (CSLA) knockout lines. Transverse stem sections of poplar 717 wild-type (WT) trees and single and double knockout lines of CSLA genes were labeled with LM21 antibody to evaluate mannan presence. Mannan was noticeably absent in both the single and double knockout lines, and it was not possible to distinguish any differences in the immunolabeling among the lines. No discernible alterations in xylan or cellulose were detected when comparing WT and knockout lines. Xylan was labeled with the CCRC-M138 antibody, while cellulose was stained with Pontamine. Bars, 100 μm. CSLA, Cellulose Synthase-Like A; KO, knockout.

to be 35.23 μg mg^{-1} of extracted tissue compared to 31.58 μg mg^{-1} present in the wild-type trees (Fig. 8; Table S9). In line 3, the content of xylose was significantly lower (P-value = 0.042), whereas in line 5, glucose was significantly higher (P-value = 0.017; Table S9). Besides line 1, which had lower amounts of rhamnose (P-value = 0.003) and galactose (P-value = 0.016), no significant differences were observed in the content of the other structural polysaccharides (Table S9). Together, these results confirm that PgCSLA1 functions as a mannan synthase capable of inducing mannan biosynthesis when ectopically expressed. Additionally, our findings demonstrate that mannan content can be increased, albeit marginally, without adversely affecting plant growth or yield.

Saccharification efficiency of mannan altered poplar stems

To evaluate the effects of altering mannan content on biomass processing, we performed a saccharification assay using two CSLA CRISPR poplar knockout lines and two overexpressing lines, one with the highest transgene expression and one with moderate overexpression of *PgCSLA1*. This experiment was performed with and without pretreatment, where the pretreatment was a dilute acid treatment (1 M HCL, 80°C, 2 h). We observed slight, but not significant, increases in glucose and xylose release (Fig. S7a,b) when comparing wild-type poplar trees with CSLA CRISPR knockouts. Notably, the poplar line with the highest ectopic overexpression of *PgCSLA1* showed the most substantial increase in glucose and xylose release (Fig. S8a,b). In general, our results show that removing mannan from poplar stems or marginally increasing its content does not have dramatic effects on biomass processing, but there may be a positive influence.

Discussion

In this study, we successfully identified CSLA genes from both poplar and spruce trees, responsible for mannan biosynthesis in woody species by combining bioinformatic analyses with *in planta* functional characterization. We demonstrated that

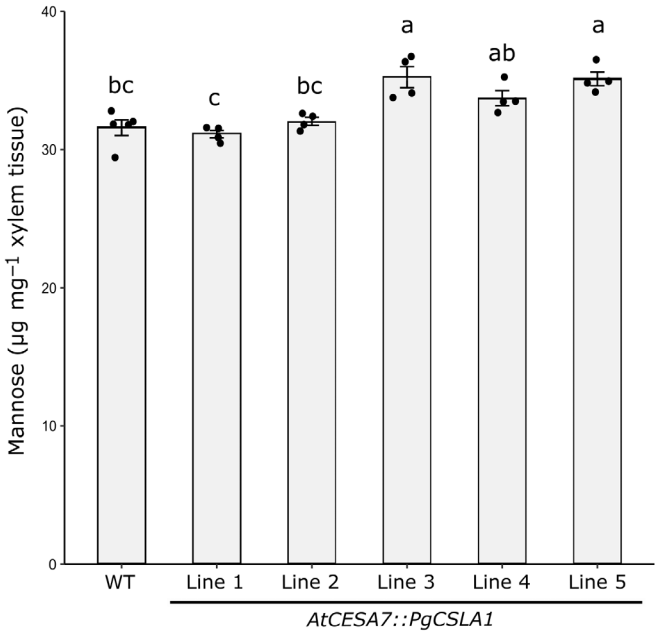

Fig. 8 Mannose composition from wild-type poplar trees and poplar lines expressing *PgCSLA1*. One-way ANOVA with a Tukey *post hoc* test was used to evaluate statistical differences (*P*-value <0.05, n = 4–5 per line, different letters indicate significant differences). Line 3 and Line 5 showed the highest mannose increase compared to the WT poplar trees. Error bars indicate the SE. WT: wild-type 717 poplar.

PtaCSLA1 from poplar and PgCSLA1 from spruce can complement the mannan-deficient Arabidopsis *csla2,3,9* triple mutant, and further that mannan content in poplar xylem can be altered without affecting plant growth. These findings provide insights into the functional roles of these proteins and their potential applications in biotechnology.

CSLA family members in poplar trees and their contribution to mannan biosynthesis

In poplar, bioinformatic analysis identified five CSLA family genes (*PtCSLA1*, *PtCSLA2*, *PtCSLA3*, *PtCSLA4*, and *PtCSLA5*) as candidates for mannan biosynthesis, with two encoding proteins shown to exhibit β-mannan synthase activity *in vitro* (PtCSLA1 and PtCSLA3; Suzuki *et al.*, 2006; Liepman *et al.*, 2007). In the current study, our phylogenetic results were consistent with those of Suzuki *et al.* (2006). We also found that the CSLA family in poplar is composed of five genes that are grouped into three different subgroups, where *PtCSLA1* and *PtCSLA2* compose one of the subgroups and have a high expression in the xylem. In our study, *PtaCSLA1* and *PtaCSLA2* corresponded to the *PtCSLA1* and *PtCSLA2* reported by Suzuki *et al.* (2006). In contrast to the expression data reported by Suzuki *et al.* (2006), we only found *PtaCSLA1* and *PtaCSLA2* to display high expression in wild-type hybrid poplar and also show significant repression in GolS overexpressing trees, whereas *PtaCSLA5* did not show high levels of expression in wild-type trees or repression in the transgenics that had substantially altered mannan content, according to Unda *et al.* (2017). In addition, we observed that *PtaCSLA1* and *PtCSLA2* were grouped with *AtCSLA3* in our phylogenetic tree instead of being grouped with *AtCSLA9*, as reported by Suzuki *et al.* (2006). The variation in result is likely due to the extended number of plant sequences employed to generate our phylogenetic tree, as Suzuki *et al.* (2006) only compared CSLA sequences from Arabidopsis, poplar, rice, and guar.

Research conducted in Arabidopsis has shown that even though several genes can be classified into a CSLA family, not necessarily all of them contribute equally to mannan production in all plant tissues. For example, in Arabidopsis, AtCSLA9 is the main contributor to mannan synthesis in stems, whereas AtCSLA2 and AtCSLA3 only produce a minor fraction of the glucomannan found in this same tissue (Goubet *et al.*, 2009). Stems of Arabidopsis *csla9* mutants have *c.* 20% of the wild-type mannose (by weight), whereas *csla2* and *csla3* double mutants have 86% (Goubet *et al.*, 2009). Despite some of the poplar CSLAs having been characterized *in vitro* (Suzuki *et al.*, 2006), our understanding of their contribution to mannan synthesis *in planta* remained limited. In the current study, we demonstrated that, when expressed *in planta*, *PtaCSLA1* can recover the mannan content of Arabidopsis mutants. In addition, we showed that when *PtaCSLA1* and *PtaCSLA2* are mutated in poplar, mannan is abolished from the xylem tissue. We also demonstrated that the mutation of *PtaCSLA1* alone is sufficient to eliminate mannan from the xylem, as both the single and double knockout lines generated via CRISPR-Cas9 were indistinguishable in mannan content. In general, our results conclusively show that PtaCSLA1 is a β-mannan synthase in poplar and provide evidence that it synthesizes non-patterned glucomannan absent of galactosyl side chains. Moreover, our results suggest that the contribution of other CSLAs to mannan biosynthesis in the xylem of poplar is likely null or negligible, suggesting PtaCSLA1 is the main contributor. Future studies should evaluate if the other CSLA encode proteins with true β-mannan synthase activity, such as *PtCSLA3*, which may be important in other stages of plant development or tissues.

CSLA family in spruce

We identified and functionally characterized one of the putative genes composing the CSLA family in spruce (*Picea engelmannii* × *glauca* × *sitchensis*), *PgCSLA1*. Although in our phylogenetic analysis we found *GCHX01322020* (*PgCSLA2*) and *GCHX01181033* (*PgCSLA3*) as potential CSLAs, we did not evaluate their functionality and hence they may also be part of the CSLA family in this gymnosperm.

The well-characterized differences in mannan abundance and composition between gymnosperms and angiosperms likely reflect distinct structural and functional adaptations in their secondary cell walls (Weng & Chapple, 2010; Spicer, 2016; Berglund *et al.*, 2020). Despite these differences, our bioinformatic analyses show that CSLA proteins in spruce maintain a high degree of sequence conservation across plant species, including the characteristic QxxRW motif. Additionally, our results also show that the CSLA family in spruce is composed of fewer CSLA genes compared to poplar, likely because of the absence of

genome duplications in this tree species. Overall, our study supports the idea of a highly conserved structure and function among the CSLA enzymes across different plant lineages.

Implications of eliminating mannan from poplar stem by mutating CSLAs

Studies examining Arabidopsis seeds have shown that alterations in mannan content impact mucilage integrity, whereas NMR studies clearly demonstrate that mannan interacts with cellulose and lignin. These findings implicate mannan in maintaining cell wall architecture (Yu *et al.*, 2018; Terrett *et al.*, 2019). In the current study, we explored how the absence of mannan affects poplar tree growth and cell wall composition. We clearly show that mannan does not appear to play an essential role in poplar growth and/or xylem development, as we did not observe significant changes in tree height, stem diameter, or total biomass in the lines where mannan was absent from poplar xylem. These results are consistent with previous reports in Arabidopsis, where the absence of mannan did not affect plant morphology or stem strength (Goubet *et al.*, 2009).

Studies in Arabidopsis have shown that when mannan is absent along with xyloglucan, mutants display exacerbated phenotypes (Yu *et al.*, 2022). For example, Arabidopsis *csla2 xxt1 xxt2* mutants manifest smaller rosette diameters and significantly shorter stems and siliques than the *xxt1 xxt2* or the *csla2* mutants alone, providing evidence for a functional connection between β-GGM and XyG (Yu *et al.*, 2022). Even though our results show that mannan by itself does not seem to play a critical role in maintaining xylem architecture, future studies should evaluate how changing mannan in concert with other hemicelluloses may impact plant growth. The tree lines created in the current study represent an excellent platform to address this question.

Similarly, mannan has been proposed as an important signaling molecule, as it has been implicated in plant development and defense (Zhao *et al.*, 2013; Zhang *et al.*, 2023). In Arabidopsis, a mutation in *At*Man6 was shown to modulate the transition between PCW and SCW formation (Zhang *et al.*, 2023). Arabidopsis *man6* mutants looked morphologically like wild-type plants but showed higher amounts of lignin, xylose, and mannose (Zhang *et al.*, 2023). In the current study, even though we did not target enzymes in the plasma membrane associated with mannan remodeling, we expected that the CRISPR-Cas9 poplar lines, lacking available mannan to generate oligosaccharides involved in signaling, would exhibit effects on growth and development. However, no such impacts were observed. Moreover, we did not find statistical differences in the cell wall composition between the wild-type and CSLA knockout lines (outside of mannan content). However, we did observe minor increases in lignin and xylose content. In general, our results suggest that the absence of mannan does not drastically affect SCW formation, suggesting that it may not be an essential signaling molecule needed for SCW deposition as previously proposed (Zhao *et al.*, 2013; Zhang *et al.*, 2023).

Mannan has been implicated in the reallocation of carbon flux during tension wood (TW) formation (Andersson-Gunnerås *et al.*, 2006; Mizrachi *et al.*, 2015). TW is produced on the upper side of branches or leaning stems in response to gravitational stimuli or mechanical stress. It is characterized by fibers containing a gelatinous cell wall layer (G-layer), which is enriched in cellulose and depleted in lignin and hemicelluloses (Mizrachi *et al.*, 2015). In addition to these compositional changes, TW typically exhibits a reduced number of vessel elements and a higher developmental rate compared to normal wood (Mizrachi *et al.*, 2015). Andersson-Gunnerås *et al.* (2006) identified genes such as putative GDP-mannose pyrophosphorylases and the currently studied *PtaCSLA1* as being downregulated in TW tissues. This downregulation has been associated with the hypothesis that carbon flux shifts from hemicellulose (e.g., mannan) biosynthesis toward increased cellulose production, possibly through enhanced use of fructose-6-phosphate (Andersson-Gunnerås *et al.*, 2006). The *PtaCSLA1/2* knockout lines generated in the present study provide a valuable tool for dissecting the role of mannans in TW formation. Specifically, they allow us to examine how the absence of mannan affects other cell wall components and whether it influences the signaling pathways or gene expression networks involved in the induction of TW.

Implications of expressing *PgCSLA1* in Arabidopsis

The production of a particular type of mannan in different plant lineages seems to be modulated by various elements (Ishida *et al.*, 2023; Yoshimi *et al.*, 2025). For example, recent studies have shown that the production of decorated mannans requires a spatiotemporal coordination of both CSLAs and mannan galactosyltransferases (Ishida *et al.*, 2023; Yoshimi *et al.*, 2025). Other factors controlling this process may also involve accessory proteins such as MSR proteins (Voiniciuc *et al.*, 2019). In the current study, we identified PgCSLA1 as one of the most plausible candidates responsible for the synthesis of the galactoglucomannan backbone in spruce. We showed that when expressed *in planta*, this gene was able to recover the Arabidopsis *csla2,3,9* triple mutant phenotype (lack of mannan), specifically increasing the content of non-patterned glucomannan to wild-type levels. In general, these results confirm that multiple factors are involved in the production of a particular type of mannan and are not uniquely CSLA dependent.

Implications of increasing mannan from poplar stems by expressing CSLAs

One of the strategies used in the current study to better understand the mannan importance in plants was to increase its content in the stems of trees via the ectopic expression of an exogenous gene, specifically in this case the spruce *PgCSLA1* gene in poplar. We demonstrated that overexpressing *PgCSLA1* in xylem is sufficient to increase mannan content and that this change does not affect plant growth or yield and does not manifest in major changes in total cell wall composition. These results are relevant for biotechnological applications aimed at increasing mannan production for industrial purposes, offering a sustainable and efficient strategy for its commercial use.

Biomass processing implications of manipulating mannan content in poplar stems

To better understand the effects of modifying mannan content on biomass processing, we performed a saccharification assay. Our results indicate that removing mannan from poplar stems only marginally affects glucose and/or xylose release. These findings are intriguing, as we imagined that removing mannan would enhance cellulose accessibility by simplifying the cell wall matrix. However, several factors could explain this outcome, including the possibility that the proportion of mannan in the cell wall is too small for its modification to have a substantial impact on sugar release. Alternatively, the absence of mannan may trigger compensatory cell wall remodeling that preserves the structural integrity of other cell chemical components, thereby mitigating any perceptible effects on enzymatic hydrolysis. Further research in this area is warranted.

Similarly, our results showed that increasing total mannan content, although marginally, did not lead to significant changes in glucose or xylose release; although slight increases were observed in one of the modified lines. Future studies should investigate whether greater increases in mannan, beyond those reported in this study, would have a significant impact on biomass processing. Overall, our findings suggest that modifying mannan content either by eliminating it or increasing it in the proportions reported is not sufficient to drastically impact saccharification efficiency in poplar. This research highlights the complexity of the interactions that maintain cell wall integrity and suggests that alternative approaches may be needed to enhance biomass processing efficiency.

In summary, we identified two functional CSLA enzymes, one from poplar, PtaCSLA1, and one from spruce, PgCSLA1. We demonstrated that these two enzymes can recover mannan content in the Arabidopsis *csla2,3,9* triple mutant that is depleted of mannan. We showed that when mutated, *PtaCSLA1* can abolish the synthesis of mannan in the xylem tissue of poplar trees without affecting tree growth. As such, we contend that *PtaCSLA1* is the primary gene responsible for mannan biosynthesis in poplar stems. Similarly, we showed that when ectopically expressed in poplar, PgCSLA1 can increase the content of mannan without affecting plant growth. We also demonstrated that reducing mannan content has marginal impacts on saccharification efficiency when using dilute acid as a pretreatment, while increasing mannan may have a minor effect on glucose and xylose release. Overall, this study demonstrates an effective approach to engineering mannan content in trees and highlights that this polysaccharide is not essential for secondary cell wall formation in poplar trees. Our work provides a platform for further studying the role of mannan in cell wall structure, as it is evolutionarily conserved, but its true function in cell walls is yet to be fully uncovered.

Acknowledgements

We thank Chung-Jui (CJ) Tsai for advice on CRISPR-Cas9 cloning, Ian Black for guidance with linkage analysis, and Ruby Hsu for assistance in the laboratory. This research was undertaken, in part, with support from the UBC Four Year Doctoral Fellowship (4YF) program.

Competing interests

None declared.

Author contributions

SGR and SM conceived the study. SGR undertook all the bioinformatic analyses, generated the Arabidopsis and poplar lines, and conducted the cell wall chemistry analyses. LdV performed the saccharification analysis and provided lab assistance. PD provided laboratory access, reagents, and equipment necessary for the PACE analyses. SGR and YY conducted the PACE analyses. SGR and EE performed the immunolabeling experiment. SGR prepared the manuscript, and all authors contributed to the final version.

ORCID

Paul Dupree https://orcid.org/0000-0001-9270-6286
Elzat Eli https://orcid.org/0009-0005-1794-335X
Sydne Guevara-Rozo https://orcid.org/0000-0002-0340-0347
Shawn D. Mansfield https://orcid.org/0000-0002-0175-554X
Lisanne de Vries https://orcid.org/0000-0002-3245-9081
Yoshihisa Yoshimi https://orcid.org/0000-0002-6734-6677

Data availability

All data supporting the findings of this study are either in the main document or contained in the Supporting Information.

References

Andersson-Gunneras S, Mellerowicz EJ, Love J, Segerman B, Ohmiya Y, Coutinho PM, Nilsson P, Henrissat B, Moritz T, Sundberg B. 2006. Biosynthesis of cellulose-enriched tension wood in *Populus*: global analysis of transcripts and metabolites identifies biochemical and developmental regulators in secondary wall biosynthesis. *The Plant Journal* **45**: 144–165.

Berglund J, Mikkelsen D, Flanagan BM, Dhital S, Gaunitz S, Henriksson G, Lindström ME, Yakubov GE, Gidley MJ, Vilaplana F. 2020. Wood hemicelluloses exert distinct biomechanical contributions to cellulose fibrillar networks. *Nature Communications* **11**: 4692.

Black I, Heiss C, Carlson RW, Azadi P. 2021. Linkage analysis of oligosaccharides and polysaccharides: a tutorial. In: Delobel A, ed. *Mass spectrometry of glycoproteins. Methods in molecular biology, vol. 2271*. New York, NY, USA: Humana, 249–271. doi: 10.1007/978-1-0716-1241-5_18.

Brinkman EK, Chen T, Amendola M, van Steensel B. 2014. Easy quantitative assessment of genome editing by sequence trace decomposition. *Nucleic Acids Research* **42**: e168.

Clough SJ, Bent AF. 1998. Floral dip: a simplified method for Agrobacterium-mediated transformation of *Arabidopsis thaliana*. *The Plant Journal* **16**: 735–743.

Coleman HD, Park J-Y, Nair R, Chapple C, Mansfield SD. 2008. RNAi-mediated suppression of *p* -coumaroyl-CoA 3′-hydroxylase in hybrid poplar impacts lignin deposition and soluble secondary metabolism. *Proceedings of the National Academy of Sciences, USA* **105**: 4501–4506.

Conklin PL, Norris SR, Wheeler GL, Williams EH, Smirnoff N, Last RL. 1999. Genetic evidence for the role of GDP-mannose in plant ascorbic acid (vitamin

C) biosynthesis. *Proceedings of the National Academy of Sciences, USA* **96**: 4198–4203.

Conklin PL, Saracco SA, Norris SR, Last RL. 2000. Identification of ascorbic acid-deficient *Arabidopsis thaliana* mutants. *Genetics* **154**: 847–856.

De Meester B, Oyarce P, Vanholme R, Van Acker R, Tsuji Y, Vangeel T, Van den Bosch S, Van Doorsselaere J, Sels B, Ralph J *et al.* 2022. Engineering curcumin biosynthesis in poplar affects lignification and biomass yield. *Frontiers in Plant Science* **13**: 943349.

Edwards M, Scott C, Gidley MJ, Reid JSG. 1992. Control of mannose/galactose ratio during galactomannan formation in developing legume seeds. *Planta* **187**: 67–74.

Glass M, Barkwill S, Unda F, Mansfield SD. 2015. Endo-β-1,4-glucanases impact plant cell wall development by influencing cellulose crystallization. *Journal of Integrative Plant Biology* **57**: 396–410.

Goubet F, Barton CJ, Mortimer JC, Yu X, Zhang Z, Miles GP, Richens J, Liepman AH, Seffen K, Dupree P. 2009. Cell wall glucomannan in Arabidopsis is synthesised by CSLA glycosyltransferases, and influences the progression of embryogenesis. *The Plant Journal* **60**: 527–538.

Goubet F, Jackson P, Deery MJ, Dupree P. 2002. Polysaccharide analysis using carbohydrate gel electrophoresis: a method to study plant cell wall polysaccharides and polysaccharide hydrolases. *Analytical Biochemistry* **300**: 53–68.

Goubet F, Misrahi A, Park SK, Zhang Z, Twell D, Dupree P. 2003. AtCSLA7, a cellulose synthase-like putative glycosyltransferase, is important for pollen tube growth and embryogenesis in Arabidopsis. *Plant Physiology* **131**: 547–557.

Grantham NJ, Wurman-Rodrich J, Terrett OM, Lyczakowski JJ, Stott K, Iuga D, Simmons TJ, Durand-Tardif M, Brown SP, Dupree R *et al.* 2017. An even pattern of xylan substitution is critical for interaction with cellulose in plant cell walls. *Nature Plants* **3**: 859–865.

Ishida K, Ohba Y, Yoshimi Y, Wilson LFL, Echevarría-Poza A, Yu L, Iwai H, Dupree P. 2023. Differing structures of galactoglucomannan in eudicots and non-eudicot angiosperms. *PLoS ONE* **18**: e0289581.

Jacobs TB, Martin GB. 2016. High-throughput CRISPR vector construction and characterization of DNA modifications by generation of tomato hairy roots. *Journal of Visualized Experiments* **110**: 53843.

Karimi M, Inzé D, Depicker A. 2002. GATEWAY™ vectors for Agrobacterium-mediated plant transformation. *Trends in Plant Science* **7**: 193–195.

Kolosova N, Miller B, Ralph S, Ellis BE, Douglas C, Ritland K, Bohlmann J. 2004. Isolation of high-quality RNA from gymnosperm and angiosperm trees. *BioTechniques* **36**: 821–824.

Krogh A, Larsson B, von Heijne G, Sonnhammer ELL. 2001. Predicting transmembrane protein topology with a hidden markov model: application to complete genomes11Edited by F. Cohen. *Journal of Molecular Biology* **305**: 567–580.

Kumar S, Stecher G, Li M, Knyaz C, Tamura K. 2018. MEGA X: molecular evolutionary genetics analysis across computing platforms. *Molecular Biology and Evolution* **35**: 1547–1549.

Lapierre C, Sibout R, Laurans F, Lesage-Descauses M-C, Déjardin A, Pilate G. 2021. *p* -Coumaroylation of poplar lignins impacts lignin structure and improves wood saccharification. *Plant Physiology* **187**: 1374–1386.

Liepman AH, Nairn CJ, Willats WGT, Sørensen I, Roberts AW, Keegstra K. 2007. Functional genomic analysis supports conservation of function among cellulose synthase-like a gene family members and suggests diverse roles of mannans in plants. *Plant Physiology* **143**: 1881–1893.

Liepman AH, Wilkerson CG, Keegstra K. 2005. Expression of cellulose synthase-like (*Csl*) genes in insect cells reveals that *CslA* family members encode mannan synthases. *Proceedings of the National Academy of Sciences, USA* **102**: 2221–2226.

Mai-Gisondi G, Maaheimo H, Chong S-L, Hinz S, Tenkanen M, Master E. 2017. Functional comparison of versatile carbohydrate esterases from families CE1, CE6 and CE16 on acetyl-4-O-methylglucuronoxylan and acetyl-galactoglucomannan. *Biochimica et Biophysica Acta (BBA) - General Subjects* **1861**: 2398–2405.

Mizrachi E, Maloney VJ, Silberbauer J, Hefer CA, Berger DK, Mansfield SD, Myburg AA. 2015. Investigating the molecular underpinnings underlying morphology and changes in carbon partitioning during tension wood formation in *Eucalyptus*. *New Phytologist* **206**: 1351–1363.

Murashige T, Skoog F. 1962. A revised medium for rapid growth and bio assays with tobacco tissue cultures. *Physiologia Plantarum* **15**: 473–497.

Nguyen L-T, Schmidt HA, von Haeseler A, Minh BQ. 2015. IQ-TREE: a fast and effective stochastic algorithm for estimating maximum-likelihood phylogenies. *Molecular Biology and Evolution* **32**: 268–274.

Nishigaki N, Yoshimi Y, Kuki H, Kunieda T, Hara-Nishimura I, Tsumuraya Y, Takahashi D, Dupree P, Kotake T. 2021. Galactoglucomannan structure of Arabidopsis seed-coat mucilage in GDP-mannose synthesis impaired mutants. *Physiologia Plantarum* **173**: 1244–1252.

Nishimura H, Kamiya A, Nagata T, Katahira M, Watanabe T. 2018. Direct evidence for α ether linkage between lignin and carbohydrates in wood cell walls. *Scientific Reports* **8**: 6538.

Pattathil S, Avci U, Miller JS, Hahn MG. 2012. Immunological approaches to plant cell wall and biomass characterization: glycome profiling. In: *Biomass conversion*. Totowa, NJ, USA: Humana Press, 61–72. doi: 10.1007/978-1-61779-956-3_6.

Rodríguez-Gacio M d C, Iglesias-Fernández R, Carbonero P, Matilla ÁJ. 2012. Softening-up mannan-rich cell walls. *Journal of Experimental Botany* **63**: 3976–3988.

Sawake S, Tajima N, Mortimer JC, Lao J, Ishikawa T, Yu X, Yamanashi Y, Yoshimi Y, Kawai-Yamada M, Dupree P *et al.* 2015. KONJAC1 and 2 are key factors for GDP-mannose generation and affect l-ascorbic acid and glucomannan biosynthesis in Arabidopsis. *Plant Cell* **27**: 3397–3409.

Saxena IM, Brown RM. 1997. Identification of cellulose synthase(s) in higher plants: sequence analysis of processive β-glycosyltransferases with the common motif 'D, D, D35Q(R,Q)XRW'. *Cellulose* **4**: 33–49.

Scheller HV, Ulvskov P. 2010. Hemicelluloses. *Annual Review of Plant Biology* **61**: 263–289.

Smith RA, Gonzales-Vigil E, Karlen SD, Park J-Y, Lu F, Wilkerson C, Samuels AL, Ralph J, Mansfield SD. 2015. Engineering monolignol p-coumarate conjugates into Poplar and Arabidopsis lignins. *Plant Physiology* **169**: 2992–3001.

Spicer R. 2016. Variation in angiosperm wood structure and its physiological and evolutionary significance. In: Groover A, Cronk Q, eds. *Comparative and evolutionary genomics of angiosperm trees*. Cham, Switzerland: Springer, 19–60. doi: 10.1007/7397_2016_28.

Suzuki S, Li L, Sun Y-H, Chiang VL. 2006. The cellulose synthase gene superfamily and biochemical functions of xylem-specific cellulose synthase-like genes in *Populus trichocarpa*. *Plant Physiology* **142**: 1233–1245.

Taylor G. 2002. Populus: Arabidopsis for forestry. do we need a model tree? *Annals of Botany* **90**: 681–689.

Terrett OM, Dupree P. 2019. Covalent interactions between lignin and hemicelluloses in plant secondary cell walls. *Current Opinion in Biotechnology* **56**: 97–104.

Terrett OM, Lyczakowski JJ, Yu L, Iuga D, Franks WT, Brown SP, Dupree R, Dupree P. 2019. Molecular architecture of softwood revealed by solid-state NMR. *Nature Communications* **10**: 4978.

Tsai C-J, Xue L-J. 2015. CRISPRing into the woods. *GM Crops & Food* **6**: 206–215.

Unda F, Kim H, Hefer C, Ralph J, Mansfield SD. 2017. Altering carbon allocation in hybrid poplar (*Populus alba* × *grandidentata*) impacts cell wall growth and development. *Plant Biotechnology Journal* **15**: 865–878.

Van Acker R, Vanholme R, Storme V, Mortimer JC, Dupree P, Boerjan W. 2013. Lignin biosynthesis perturbations affect secondary cell wall composition and saccharification yield in *Arabidopsis thaliana*. *Biotechnology for Biofuels* **6**: 46.

Voiniciuc C. 2022. Modern mannan: a hemicellulose's journey. *New Phytologist* **234**: 1175–1184.

Voiniciuc C, Dama M, Gawenda N, Stritt F, Pauly M. 2019. Mechanistic insights from plant heteromannan synthesis in yeast. *Proceedings of the National Academy of Sciences, USA* **116**: 522–527.

Voiniciuc C, Schmidt MH-W, Berger A, Yang B, Ebert B, Scheller HV, North HM, Usadel B, Günl M. 2015. MUCILAGE-RELATED10 produces galactoglucomannan that maintains pectin and cellulose architecture in Arabidopsis seed mucilage. *Plant Physiology* **169**: 403–420.

Wang Y, Mortimer JC, Davis J, Dupree P, Keegstra K. 2013. Identification of an additional protein involved in mannan biosynthesis. *The Plant Journal* **73**: 105–117.

Weng J, Chapple C. 2010. The origin and evolution of lignin biosynthesis. *New Phytologist* **187**: 273–285.

Wilkerson CG, Mansfield SD, Lu F, Withers S, Park J-Y, Karlen SD, Gonzales-Vigil E, Padmakshan D, Unda F, Rencoret J *et al.* 2014. Monolignol ferulate transferase introduces chemically labile linkages into the lignin backbone. *Science* **344**: 90–93.

Wise AA, Liu Z, Binns AN. 2006. Three methods for the introduction of foreign DNA into Agrobacterium. In: Wang K, ed. *Agrobacterium protocols, 2nd edn, vol. 343*. Totowa, NJ, USA: Humana Press, 43–54.

Yoshimi Y, Yu L, Cresswell R, Guo X, Echevarría-Poza A, Lyczakowski JJ, Dupree R, Kotake T, Dupree P. 2025. Glucomannan engineering highlights roles of galactosyl modification in fine-tuning cellulose-glucomannan interaction in Arabidopsis cell walls. *Nature Communications* **16**: 1235.

Yu L, Lyczakowski JJ, Pereira CS, Kotake T, Yu X, Li A, Mogelsvang S, Skaf MS, Dupree P. 2018. The patterned structure of galactoglucomannan suggests it may bind to cellulose in seed mucilage. *Plant Physiology* **178**: 1011–1026.

Yu L, Shi D, Li J, Kong Y, Yu Y, Chai G, Hu R, Wang J, Hahn MG, Zhou G. 2014. CELLULOSE SYNTHASE-LIKE A2, a glucomannan synthase, is involved in maintaining adherent mucilage structure in Arabidopsis seed. *Plant Physiology* **164**: 1842–1856.

Yu L, Yoshimi Y, Cresswell R, Wightman R, Lyczakowski JJ, Wilson LFL, Ishida K, Stott K, Yu X, Charalambous S *et al.* 2022. Eudicot primary cell wall glucomannan is related in synthesis, structure, and function to xyloglucan. *Plant Cell* **34**: 4600–4622.

Zhang R, Li B, Zhao Y, Zhu Y, Li L. 2023. An essential role for mannan degradation in both cell growth and secondary cell wall formation. *Journal of Experimental Botany* **75**: 1407–1420.

Zhang X, Henriques R, Lin S-S, Niu Q-W, Chua N-H. 2006. *Agrobacterium*-mediated transformation of *Arabidopsis thaliana* using the floral dip method. *Nature Protocols* **1**: 641–646.

Zhao Y, Song D, Sun J, Li L. 2013. Populus endo-beta-mannanase PtrMAN6 plays a role in coordinating cell wall remodeling with suppression of secondary wall thickening through generation of oligosaccharide signals. *The Plant Journal* **74**: 473–485.

Zhong R, Cui D, Ye Z-H. 2018. Members of the DUF231 family are O-acetyltransferases catalyzing 2-O- and 3-O-acetylation of mannan. *Plant and Cell Physiology* **59**: 2339–2349.

Supporting Information

Additional Supporting Information may be found online in the Supporting Information section at the end of the article.

Dataset S1 *Potri.008G026400* transcript sequence from poplar 717.

Fig. S1 Multiple sequence alignment of Arabidopsis CSLAs and the putative CSLAs from poplar and spruce.

Fig. S2 Linkage analysis of *csla2,3,9 PgCSLA1*-complemented lines.

Fig. S3 Mannan backbone structure in *csla2,3,9 PtaCSLA1*-complemented lines digested with *An*GH5.

Fig. S4 Mannan backbone structure in *csla2,3,9 PgCSLA1*-complemented lines digested with *An*GH5.

Fig. S5 CRISPR Cas9 knockouts of poplar CSLA genes.

Fig. S6 Expression of *PgCSLA1* in poplar lines carrying the *AtCESA7::PgCSLA1* construct.

Fig. S7 Glucose and xylose release from limited saccharification assays in CSLA CRISPR knockout poplar lines.

Fig. S8 Glucose and xylose release from limited saccharification assays in poplar lines expressing *PgCSLA1*.

Table S1 Primers used for the CSLA gene candidates, CRISPR cloning, and qPCR.

Table S2 Total transmembrane domains in CSLAs of Arabidopsis and the putative CSLAs of poplar and spruce.

Table S3 Expression of CSLA poplar candidate genes.

Table S4 Structural polysaccharide composition of Arabidopsis WT plants, *csla2,3,9* triple mutants, and *csla2,3,9* mutants complemented with *AtCESA7::PtaCSLA1*.

Table S5 Structural polysaccharide composition of Arabidopsis WT plants, *csla2,3,9* triple mutants, and *csla2,3,9* mutants complemented with *CESA7::PgCSLA1*.

Table S6 Summary of mutations observed in single and double poplar CRISPR Cas9 knockout lines.

Table S7 Mean growth measurements and lignin content of single and double poplar CSLA knockout lines.

Table S8 Mean growth measurements and lignin content of transgenic poplar lines expressing *PgCSLA1*.

Table S9 Structural cell wall carbohydrates of poplar lines expressing *PgCSLA1*.

Please note: Wiley is not responsible for the content or functionality of any Supporting Information supplied by the authors. Any queries (other than missing material) should be directed to the *New Phytologist* Central Office.